

## Generation of modulated magnetic structures based on cluster multipole expansion: Application to $\alpha$ -Mn and $\text{CoM}_3\text{S}_6$

Yuki Yanagi,<sup>1,2</sup> Hiroaki Kusunose<sup>3,4</sup>, Takuya Nomoto<sup>5</sup>, Ryotaro Arita<sup>5,6</sup> and Michi-To Suzuki<sup>1,7</sup>

<sup>1</sup>Center for Computational Materials Science, Institute for Materials Research, Tohoku University, Sendai, Miyagi 950-8577, Japan

<sup>2</sup>Liberal Arts and Sciences, Toyama Prefectural University, Imizu, Toyama 939-0398, Japan


<sup>3</sup>Department of Physics, Meiji University, Kawasaki 214-8571, Japan

<sup>4</sup>The Institute for Solid State Physics, The University of Tokyo, Kashiwanoha 5-1-5, Chiba 277-8581, Japan

<sup>5</sup>Research Center for Advanced Science and Technology, University of Tokyo, Komaba Meguro-ku, Tokyo 153-8904, Japan

<sup>6</sup>Center for Emergent Matter Science, RIKEN, Wako, Saitama 351-0198, Japan

<sup>7</sup>Center for Spintronics Research Network, Graduate School of Engineering Science, Osaka University, Toyonaka, Osaka 560-8531, Japan

 (Received 28 February 2022; revised 6 November 2022; accepted 4 December 2022; published 10 January 2023)

We present a systematic method to automatically generate symmetry-adapted magnetic structures for a given crystal structure and general propagation vector  $\mathbf{k}$  as an efficient approach of the analysis of complex modulated magnetic structures. The method is developed as an extension of the generation scheme based on the multipole expansion, which was demonstrated only for the propagation vector  $\mathbf{k} = \mathbf{0}$  [M.-T. Suzuki *et al.*, *Phys. Rev. B* **99**, 174407 (2019)]. The symmetry-adapted magnetic structures characterized with an ordering vector  $\mathbf{k}$  are obtained by mapping the multipole magnetic alignments on a virtual cluster to the periodic crystal structure with the phase factor for the wave vector  $\mathbf{k}$ . This method provides all magnetic bases compatible with irreducible representations under a  $\mathbf{k}$  group for a given crystal structure and wave vector  $\mathbf{k}$ . Multiple- $\mathbf{k}$  magnetic structures are derived from a superposition of single- $\mathbf{k}$  magnetic bases related to the space group symmetry. We apply the scheme to deduce the magnetic structures of  $\alpha$ -Mn and  $\text{CoM}_3\text{S}_6$  ( $M = \text{Nb}, \text{Ta}$ ), in which the large anomalous Hall effect has recently been observed in antiferromagnetic phases, and identify the magnetic structures inducing anomalous Hall effect without net magnetization. The physical phenomena originating from emergent multipoles in the ordered phases are also discussed based on the Landau theory.

DOI: [10.1103/PhysRevB.107.014407](https://doi.org/10.1103/PhysRevB.107.014407)

### I. INTRODUCTION

Magnetic materials with complexly arranged magnetic moments in crystal provide a platform for exploring various exotic phenomena and potential device applications. The details of magnetic structures play a crucial role for intriguing physical phenomena, such as the anomalous/topological Hall effect, nonreciprocal charge transport, and magnetoelectric effect. Therefore the characterization of magnetic structures is a key to understanding such physical phenomena in magnetically ordered phases.

A systematic generation and characterization scheme of symmetry-adapted basis set based on the multipole expansion combined with group theory has been proposed in our previous studies [1,2]. In this method, the multipole expansion for macroscopic electromagnetic fields is extended to describe the configuration of magnetic moments in general magnetic orderings using multipolar moments with irreducible representations (IRREPs) under crystallographic point group. This enables us with an efficient analysis of electronic properties and macroscopic responses in antiferromagnets. It has been elucidated that the magnetic structure in a noncollinear antiferromagnet  $\text{Mn}_3\text{Sn}$  can be viewed as a magnetic octupole with use of this method [1,3]. The magnetic octupole scenario provides a unified understanding of anomalous responses in

$\text{Mn}_3\text{Sn}$  such as the large anomalous Hall effect (AHE) [4], anomalous Nernst effect (ANE) [5], and magneto-optical Kerr effect (MOKE) [6]. The analysis based on multipoles deepens insights into AHE, ANE, and MOKE beyond the conventional understanding that these phenomena are induced by net magnetization with spin-orbit coupling [7].

There are also advantages of using symmetry-classified magnetic structures in respect to prediction for stable and/or metastable magnetic states. Many experimental studies imply that most of magnetic structures are specified by a small number of IRREP [8], which classify possible transformation property of magnetic structures for the space group operation of crystal [9–11]. Actually, the recent benchmark calculation using a high-throughput prediction scheme of magnetic structure making use of the multipole expansion shows that the symmetrically classified magnetic structures are efficient candidate of initial magnetic structures employed in the first-principles calculations for given crystal structures [12].

In our magnetic structure generation method proposed previously [1,2,12], we only considered magnetic structures which have no spatial modulation over an interunit cell, that is, magnetic structures having propagation vector  $\mathbf{k} = \mathbf{0}$ . Meanwhile, many of attracting magnetic structures such as a helical magnetic order, a spin density wave, and skyrmion crystals

have finite propagation vector  $\mathbf{k}$  [13]. In this paper, we develop a generation scheme of symmetry-adapted magnetic structures with interunit cell spatial modulation quantified by propagation vector  $\mathbf{k}$ , along the line of the scheme proposed in Refs. [1,2]. Our algorithm based on the multipole expansion largely reduces the degree of freedom of generated magnetic structures and efficiently provides magnetic structures symmetrically adapted to the crystal structures with getting around under- and overgeneration of basis set that produces too few or too many basis vectors [14,15]. The method paves a way to explore the intricate magnetic structure by making full use of symmetry information.

In Sec. II, we provide general formulation of the generation scheme of symmetry adapted magnetic structures with finite  $\mathbf{k}$  vectors. We introduce the multipole expansion of the magnetic structure on an atomic cluster in Sec. II A and discuss how to define the virtual atomic cluster on which the multipole expansion is defined in Sec. II B. We then show how to generate symmetry adapted magnetic structures with single wave vector (Sec. II C) and with multiple wave vectors (Sec. II D). We further discuss possible magnetic structures of  $\alpha$ -Mn and  $\text{CoM}_3\text{S}_6$  ( $M = \text{Nb}, \text{Ta}$ ), which are known to exhibit large anomalous Hall responses in the antiferromagnetic (AFM) phases, by applying the generation scheme of magnetic structures in Sec. III. Finally, we summarize the paper and give a future perspective for design of magnetic materials in Sec. IV.

## II. METHODS

### A. Multipole expansion

We first review the multipole expansion of vector potential  $\mathbf{A}(\mathbf{r})$  and its application to magnetic structure introduced in Ref. [2]. As is well known, a spatial distribution of vector potential  $\mathbf{A}(\mathbf{r})$  outside its sources is systematically characterized by magnetic (M) and magnetic toroidal (MT) multipole moments,  $M_{lm}$  and  $T_{lm}$ , as follows [16–18]:

$$\mathbf{A}(\mathbf{r}) = \sum_{lm} \left[ \sqrt{\frac{4\pi(l+1)}{(2l+1)l}} M_{lm} \frac{\mathbf{Y}_{lm}^l(\hat{\mathbf{r}})}{r^{l+1}} - \sqrt{4\pi(l+1)} T_{lm} \frac{\mathbf{Y}_{lm}^{l+1}(\hat{\mathbf{r}})}{r^{l+2}} \right], \quad (1)$$

where the Coulomb gauge  $\nabla \cdot \mathbf{A}(\mathbf{r}) = 0$  is imposed and  $\mathbf{Y}_{lm}^{l'}(\hat{\mathbf{r}})$  ( $l \geq 1, -l \leq m \leq l, l' = l-1, l, l+1$ ) represents the vector spherical harmonics with  $\hat{\mathbf{r}} = \mathbf{r}/r$  [19,20]. The M and MT multipole moments are given as

$$M_{lm} = \sum_j \left( \frac{2I_j}{l+1} + \sigma_j \right) \cdot \mathbf{O}_{lm}(\mathbf{r}_j), \quad (2)$$

$$T_{lm} = \sum_j \left\{ \frac{\mathbf{r}_j}{l+1} \times \left( \frac{2I_j}{l+2} + \sigma_j \right) \right\} \cdot \mathbf{O}_{lm}(\mathbf{r}_j), \quad (3)$$

with

$$\mathbf{O}_{lm}(\mathbf{r}) = \sqrt{\frac{4\pi}{2l+1}} \nabla [r^l Y_{lm}^*(\hat{\mathbf{r}})], \quad (4)$$

where  $I_j$  ( $\sigma_j$ ) and  $\mathbf{r}_j$  are orbital (spin) angular momentum and position vector of each electron, respectively, and  $\nabla(r^l Y_{lm}) =$

$r^{l-1} \sqrt{l(2l+1)} \mathbf{Y}_{lm}^{l-1}$  with parity for spatial inversion  $(-1)^{l+1}$ . We define M- and MT-multipole moments in an atomic cluster by replacing the electron coordinate  $\mathbf{r}_j$  by atomic coordinate of  $j$ th atom  $\xi_j$  and neglecting the orbital magnetic moment in Eqs. (2) and (3) as discussed in Refs. [2,21]. Here and hereafter, the electric (E), M, electric toroidal (ET), and MT multipoles are denoted by  $Q$ ,  $M$ ,  $G$ , and  $T$ , respectively according to the notations in Ref. [22]. Taking into consideration that the atomic cluster is not invariant under continuous rotation but have a point group symmetry, the magnetic bases  $\psi_{l\Gamma\gamma}^{(X)}$  on the cluster characterized by symmetry-adapted multipole moments are obtained as follows:

$$\begin{aligned} \psi_{l\Gamma\gamma}^{(X)} &= \sum_{j=1}^N \sum_{\mu=x,y,z} u_{l\Gamma\gamma,j\mu}^{(X)} \mathbf{e}_{j\mu}^{\text{axial}} \\ &= \sum_{j=1}^N \mathbf{u}_{l\Gamma\gamma,j}^{(X)} \cdot \mathbf{e}_j^{\text{axial}} \quad (X = M, T), \end{aligned} \quad (5)$$

where  $\mathbf{e}_{j\mu}^{\text{axial}}$  denotes the axial unit vector located on  $j$ th atom along  $\mu (= x, y, z)$  direction with odd parity under time-reversal operation. Each magnetic basis  $\psi_{l\Gamma\gamma}^{(X)}$  is defined as  $3N$ -dimensional vector. The coefficients  $u_{l\Gamma\gamma,j\mu}^{(X)}$  are given as follows:

$$\mathbf{u}_{l\Gamma\gamma,j}^{(M)} = \mathcal{O}_{l\Gamma\gamma}(\xi_j), \quad (6)$$

$$\mathbf{u}_{l\Gamma\gamma,j}^{(T)} = \frac{1}{l+1} \mathcal{O}_{l\Gamma\gamma}(\xi_j) \times \xi_j, \quad (7)$$

where  $\Gamma$  and  $\gamma$  represent IRREPs of point group and its component, respectively and  $\mathcal{O}_{l\Gamma\gamma}$  is obtained by replacing  $Y_{lm}$  in Eq. (4) by symmetry-adapted function with  $\Gamma$ -IRREP in the point group of a given atomic cluster, which can be represented as linear combination of  $Y_{lm}$  with fixed rank  $l$ . For instance, if we replace  $Y_{2m}$  by  $\mathcal{Y}_{\Gamma\gamma} \propto x^2 - y^2 \propto Y_{2-2} + Y_{22}$ , we obtain M (MT)-multipole  $\mathbf{u}_{l\Gamma\gamma,j}^{(X)}$  ( $X = M, l = 2, \Gamma = B_{1u}$ ) [ $(X = T, l = 2, \Gamma = B_{1g})$ ] with one-dimensional  $B_{1u}$  ( $B_{1g}$ )-IRREP under  $D_{4h}$  point group.

### B. Virtual atomic cluster for the multipole expansion

We formulated schemes to generate symmetry-adapted orthogonal magnetic structures without spacial modulation of the alignment, i.e.,  $\mathbf{k} = \mathbf{0}$ , in earlier works [1,2]. In the method, we first define a virtual cluster consisting of nonoverlapped atoms related to each other by the rotation operations of the crystallographic point group. The crystallographic point group  $\mathcal{P}$  is defined as

$$\mathcal{P} = \sum_{i=1}^{N_{\text{coset}}} \{p_i | \mathbf{0}\} \mathcal{H}, \quad (8)$$

for the space group  $\mathcal{G}$  given as follows:

$$\mathcal{G} = \sum_{i=1}^{N_{\text{coset}}} \{p_i | \boldsymbol{\tau}_i\} \mathcal{HT}, \quad (9)$$

where  $p_i$  represents the point group operation with  $p_1 = E$  being identity operation,  $\boldsymbol{\tau}_i$  denotes nonprimitive translation with  $\boldsymbol{\tau}_1 = \mathbf{0}$  and  $\boldsymbol{\tau}_i \neq \mathbf{0}$  ( $i \geq 2$ ), and  $\mathcal{T}$  is the translation

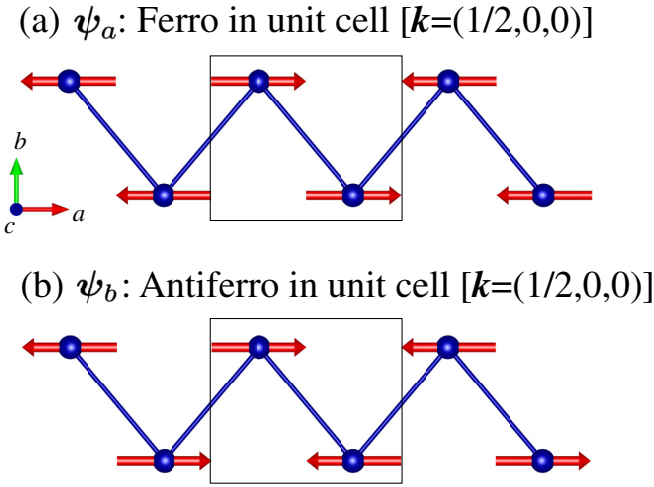
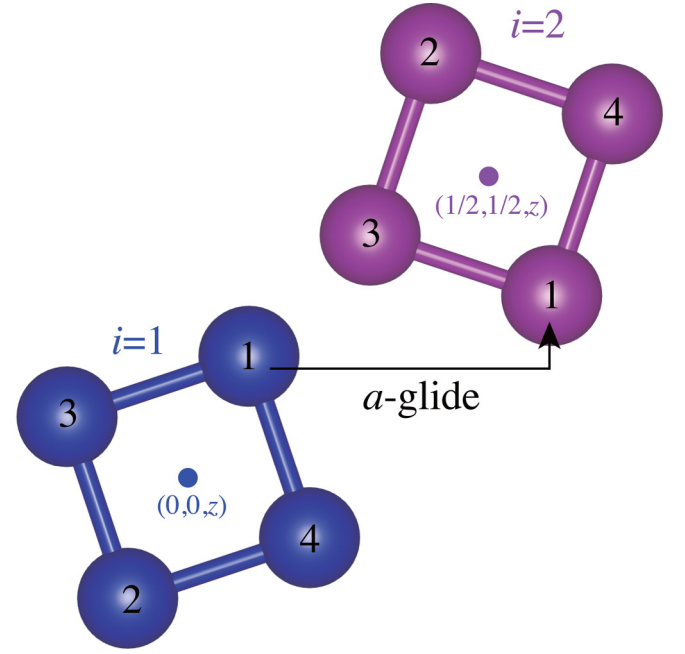


FIG. 1. (a) Ferromagnetic and (b) antiferromagnetic structures in the unit cell with  $\mathbf{k} = (\frac{1}{2}, 0, 0)$  on a zigzag chain.

group. The subgroup of the space group  $\mathcal{H}$  is composed only of the rotational operations of the space group, i.e.,  $\{h_\zeta|\mathbf{0}\} \in \mathcal{H} \subset \mathcal{G}$ , with  $h_1 = E$  ( $\zeta = 1, 2, \dots, N_h$ ). In Ref. [2], a virtual cluster is composed of  $N_0 \equiv N_{\text{coset}}N_h$  sites whose positions are defined by operating point group operations  $p_i h_\zeta$  ( $i = 1, 2, \dots, N_{\text{coset}}$ ,  $\zeta = 1, 2, \dots, N_h$ ) on a position vector  $\mathbf{r} = \mathbf{r}_1$  to classify magnetic structures having  $\mathbf{k} = \mathbf{0}$  according to the IRREPs of point group. For the case of finite propagation vector  $\mathbf{k}$ , there are specific IRREPs which are not equivalent to IRREPs in the point group symmetry of  $\mathbf{k}$  group at the Brillouin zone boundary, associated with sublattice degrees of freedom by nonsymmorphic space group operations [11,23,24]. For instance, the magnetic structures on zigzag chain with  $\mathbf{k} = (\frac{1}{2}, 0, 0)$  shown in Figs. 1(a) and 1(b) are obviously equivalent each other. Note that zigzag structure has symmetry operations shown in Table I and the  $\mathbf{k}$ -point group at  $\mathbf{k} = (\frac{1}{2}, 0, 0)$  is  $D_{2h}$ . The magnetic structures shown in Figs. 1(a) and 1(b) are transformed to each other by symmetry operations  $\{C_{2y}|(\frac{1}{2}, 0, 0)\}$ ,  $\{C_{2x}|(\frac{1}{2}, 0, 0)\}$ ,  $\{IC_{2y}|(\frac{1}{2}, 0, 0)\}$ , and  $\{IC_{2x}|(\frac{1}{2}, 0, 0)\}$  according to Table I. The other independent magnetic bases, in which the magnetic moments are directed along  $b$  and  $c$  axes, have similar transformation properties. Therefore these magnetic structures form two-dimensional IRREPs inequivalent to the IRREPs of  $D_{2h}$  point group, all of which are one-dimensional. In this case, we cannot

TABLE I. Representative elements for space group in zigzag chain and transformation properties of magnetic structures shown in Figs. 1, where  $\psi_a$  and  $\psi_b$  denote magnetic states in Figs. 1(a) and 1(b), respectively. The nonprimitive translation  $\tau$  is given by  $\tau = (\frac{1}{2}, 0, 0)$ .

	$\{E \mathbf{0}\}$	$\{C_{2z} \mathbf{0}\}$	$\{C_{2y} \tau\}$	$\{C_{2x} \tau\}$
$\psi_a$	$\psi_a$	$-\psi_a$	$\psi_b$	$-\psi_b$
$\psi_b$	$\psi_b$	$\psi_b$	$\psi_a$	$\psi_a$
	$\{I \mathbf{0}\}$	$\{IC_{2z} \mathbf{0}\}$	$\{IC_{2y} \tau\}$	$\{IC_{2x} \tau\}$
$\psi_a$	$\psi_a$	$-\psi_a$	$\psi_b$	$-\psi_b$
$\psi_b$	$-\psi_b$	$-\psi_b$	$-\psi_a$	$-\psi_a$



$$P4bm = \{E|\mathbf{0}\}\mathcal{HT} + \frac{\{IC_{2y}|\tau\}\mathcal{HT}}{a\text{-glide}}, \quad \left[ \tau = \left( \frac{1}{2}, \frac{1}{2}, 0 \right) \right]$$

$$\mathcal{H} = (\{E|\mathbf{0}\}, \{C_{2z}|\mathbf{0}\}, \{C_{4z}|\mathbf{0}\}, \{C_{4z}^{-1}|\mathbf{0}\})$$

FIG. 2. Virtual clusters in space group  $P4bm$ .

directly apply the generation scheme using virtual cluster for  $\mathbf{k} = \mathbf{0}$  constructed according to point group operations. To address this issue, we define  $N_{\text{coset}}$ -virtual clusters of which each cluster consists of  $N_h$  atoms for the magnetic structure generation for a finite propagation vector  $\mathbf{k}$  as discussed below.

### C. Magnetic structure generation for single- $\mathbf{k}$ states

We first focus on single- $\mathbf{k}$  magnetic structure, whose periodicity is characterized by a single wave vector  $\mathbf{k}$ . At a given wave vector  $\mathbf{k}$ , the magnetic bases are classified into the IRREPs of the little group of  $\mathbf{k}$  denoted as  $\mathcal{G}_k$ . The group elements in  $\mathcal{G}_k$  are composed of a subset of symmetry operations in  $\mathcal{G}$  which keeps  $\mathbf{k}$  invariant under transformations.  $\mathcal{G}_k$  is thus a subgroup of a space group  $\mathcal{G}$ . We construct the  $N_{\text{coset}}$ -virtual clusters, where each of them have  $N_h$  atoms. By operating group elements  $\{p_i|\tau_i\}h_\zeta$  ( $i = 1, 2, \dots, N_{\text{coset}}$ ,  $\zeta = 1, 2, \dots, N_h$ ) on a position vector  $\mathbf{r}_1$ , we can obtain  $i$ th virtual cluster in which  $\zeta$ th atom is indexed by  $i_\zeta$  and the internal coordinates of  $i_\zeta$ th atom is  $\tilde{\mathbf{r}}_{i_\zeta} = p_i h_\zeta \mathbf{r}_1 + \tau_i$ , where  $\tilde{\mathbf{r}}_{i_\zeta} = \mathbf{r}_1$  for  $i = 1$  and  $\zeta = 1$  [25]. Note that  $\mathbf{r}_1$  should be set to a position off the symmetry axes and planes in this procedure. For clarity of this construction, virtual clusters in space group  $P4bm$  are shown in Fig. 2 as an example. There are two sets of virtual clusters in this case, each of which consists of four atoms in square lattice arrangement since space group  $P4bm$  is decomposed as  $P4bm = \{E|\mathbf{0}\}\mathcal{HT} + \{IC_{2y}|\tau\}\mathcal{HT}$  with  $\mathcal{H} = (\{E|\mathbf{0}\}, \{C_{2z}|\mathbf{0}\}, \{C_{4z}|\mathbf{0}\}, \{C_{4z}^{-1}|\mathbf{0}\})$  and  $\tau = (\frac{1}{2}, \frac{1}{2}, 0)$ .

To take account of the interunit cell spatial modulation characterized by a propagation vector  $\mathbf{k}$ , we consider the Fourier transform of magnetic bases as follows:

$$\boldsymbol{\psi}_{\mathbf{k}l\Gamma_s\gamma_s i}^{(X)} = \frac{1}{\sqrt{N}} \sum_{\mathbf{R}} \boldsymbol{\psi}_{\mathbf{R}l\Gamma_s\gamma_s i}^{(X)} e^{i\mathbf{k}\cdot\mathbf{R}}, \quad (10)$$

$$\tilde{\mathbf{e}}_{\mathbf{k}i_\zeta}^{\text{axial}} = \frac{1}{\sqrt{N}} \sum_{\mathbf{R}} \tilde{\mathbf{e}}_{\mathbf{R}i_\zeta}^{\text{axial}} e^{i\mathbf{k}\cdot\mathbf{R}}, \quad (11)$$

where  $\tilde{\mathbf{e}}_{\mathbf{R}i_\zeta}^{\text{axial}}$  is the axial unit vector located on the site  $i_\zeta$  of virtual cluster with position  $\tilde{\boldsymbol{\eta}}_{i_\zeta} + \mathbf{R}$ , and  $\mathbf{R}$  is the primitive translation vector assuming that the virtual clusters are periodically arranged.  $\boldsymbol{\psi}_{\mathbf{R}l\Gamma_s\gamma_s i}$  are magnetic bases on the  $i$ th virtual cluster whose centers are located on  $\mathbf{R} + \boldsymbol{\tau}_i$  given as follows:

$$\boldsymbol{\psi}_{\mathbf{R}l\Gamma_s\gamma_s i}^{(X)} = \sum_{\zeta=1}^{N_h} \mathbf{u}_{l\Gamma_s\gamma_s i, \zeta}^{(X)} \cdot \tilde{\mathbf{e}}_{\mathbf{R}i_\zeta}^{\text{axial}}, \quad (12)$$

where  $\Gamma_s$  and  $\gamma_s$  represent IRREP of point group of a virtual cluster and its component, respectively. The coefficient  $\mathbf{u}_{l\Gamma_s\gamma_s i, \zeta}^{(X)}$  is obtained by putting  $p_i h_\zeta \mathbf{r}_1$  into  $\boldsymbol{\xi}_j$  in Eqs. (6) and (7). We can construct the complex basis vectors having IRREPs under  $\mathbf{k}$  group as linear combinations of the magnetic bases of Eq. (10) as follows:

$$\begin{aligned} \tilde{\boldsymbol{\Psi}}_{l\Gamma_k\gamma}^{(X)} &= \sum_{i=1}^{N_{\text{coset}}} \sum_{\Gamma_s\gamma_s} C_{kl\Gamma_s\gamma_s i; \Gamma_k\gamma}^{(X)} \boldsymbol{\psi}_{\mathbf{k}l\Gamma_s\gamma_s i}^{(X)} \\ &= \sum_{i=1}^{N_{\text{coset}}} \sum_{\zeta=1}^{N_h} \mathbf{u}_{l\Gamma_k\gamma, i, \zeta}^{(X)} \cdot \tilde{\mathbf{e}}_{\mathbf{k}i_\zeta}^{\text{axial}}, \end{aligned} \quad (13)$$

where  $\Gamma_k$  denotes the IRREPs of  $\mathbf{k}$  group,  $\gamma$  represents its component,  $\mathbf{u}_{l\Gamma_k\gamma, \alpha\mu}^{(X)}$  is given as follows:

$$\mathbf{u}_{l\Gamma_k\gamma, i, \zeta}^{(X)} = \sum_{\Gamma_s\gamma_s} C_{l\Gamma_s\gamma_s i; \Gamma_k\gamma}^{(X)} \mathbf{u}_{l\Gamma_s\gamma_s i, \zeta}^{(X)}. \quad (14)$$

Note that coefficients  $C_{l\Gamma_s\gamma_s i; \Gamma_k\gamma}$  can be obtained using ordinary projection operator method to obtain the linear combination of atomic orbitals (LCAO) for the tight-binding model with the wave vector  $\mathbf{k}$  and IRREP  $\Gamma_s$  at site  $i$  [23]. The complex magnetic basis  $\tilde{\boldsymbol{\Psi}}_{l\Gamma_k\gamma}^{(X)}$  in crystallographic systems can be obtained by mapping  $\tilde{\boldsymbol{\Psi}}_{l\Gamma_k\gamma}^{(X)}$  onto crystallographic lattices as follows:

$$\boldsymbol{\Psi}_{l\Gamma_k\gamma}^{(X)} = \sum_{i=1}^{N_{\text{coset}}} \sum_{\zeta=1}^{N_h} e^{-i\varphi_{i_\zeta}^{k,1}} \mathbf{u}_{l\Gamma_k\gamma, i, \zeta}^{(X)} \cdot \mathbf{e}_{\mathbf{k}s_{i_\zeta}[1]}^{\text{axial}}, \quad (15)$$

where  $\mathbf{e}_{\mathbf{k}\alpha}^{\text{axial}}$  represents the Fourier component of axial unit vector on site  $\alpha$  in the crystallographic system and  $s_{i_\zeta}[\alpha]$  is the permutation operator for indices of atomic sites  $\alpha$  associated with the symmetry operation  $\{p_i h_\zeta | \boldsymbol{\tau}_i\}$ , which transforms an atomic site of crystallographic system  $\boldsymbol{\eta}_\alpha$  as follows:  $\{p_i h_\zeta | \boldsymbol{\tau}_i\} \boldsymbol{\eta}_\alpha = \boldsymbol{\eta}_{s_{i_\zeta}[\alpha]} + \mathbf{R}_{i_\zeta}^\alpha$  with  $\mathbf{R}_{i_\zeta}^\alpha$  being a primitive translation vector.  $\alpha = 1$  represents the atom mapped from an atom in virtual cluster with  $i = 1$  and  $\zeta = 1$ . There is arbitrariness for the choices of  $\mathbf{r}_1$  and the atom in a unit cell of crystal system firstly mapped from an atom of virtual cluster, but the symmetry property does not depend on their choices. Transformation properties of atomic sites on  $2b$  site

TABLE II. Atomic indices transformed by representative elements for space group  $P4bm$ .

	$\{E \mathbf{0}\}$	$\{C_{2z} \mathbf{0}\}$	$\{C_{4z} \mathbf{0}\}$	$\{C_{4z}^{-1} \mathbf{0}\}$
$i$	1	1	1	1
$\zeta$	1	2	3	4
$s_{i_\zeta}[1]$	1	1	2	2
$s_{i_\zeta}[2]$	2	2	1	1
	$\{IC_{2y} \boldsymbol{\tau}\}$	$\{IC_{2x} \boldsymbol{\tau}\}$	$\{IC_{2[110]} \boldsymbol{\tau}\}$	$\{IC_{2[1\bar{1}0]} \boldsymbol{\tau}\}$
$i$	2	2	2	2
$\zeta$	1	2	3	4
$s_{i_\zeta}[1]$	2	2	1	1
$s_{i_\zeta}[2]$	1	1	2	2

in space group  $P4bm$  are shown in Table II and Fig. 3 as an example. The phase factor  $\varphi_{i_\zeta}^{k, \alpha}$  is given as  $\varphi_{i_\zeta}^{k, \alpha} = \mathbf{k} \cdot \mathbf{R}_{i_\zeta}^\alpha$ . We note that letting  $N_{\text{atom}}$  be the number of magnetic atoms in the crystallographic unit cell, each magnetic basis  $\boldsymbol{\Psi}_{l\Gamma_k\gamma}^{(X)}$  in Eq. (15) is  $3N_{\text{atom}}$ -dimensional vector while  $\tilde{\boldsymbol{\Psi}}_{l\Gamma_k\gamma}^{(X)}$  in Eq. (13) is  $3N_0$ -dimensional one with  $N_0 \geq N_{\text{atom}}$ . The magnetic bases in Eq. (15) have transformation properties of IRREP  $\Gamma_k$  in  $\mathbf{k}$ -group  $\mathcal{G}_k$  as shown in Appendix. We can obtain complete orthogonal symmetry-adapted magnetic structure basis set iteratively using Eqs. (6), (7), and (12)–(15) combined with the following Gram-Schmidt orthogonalization increasing rank  $l$  from  $l = 1$  [2],

$$\Phi_{11}^{(1)} \equiv \frac{\boldsymbol{\Psi}_{11}^{(1)}}{\sqrt{\boldsymbol{\Psi}_{11}^{(1)*} \cdot \boldsymbol{\Psi}_{11}^{(1)}}}, \quad (16)$$

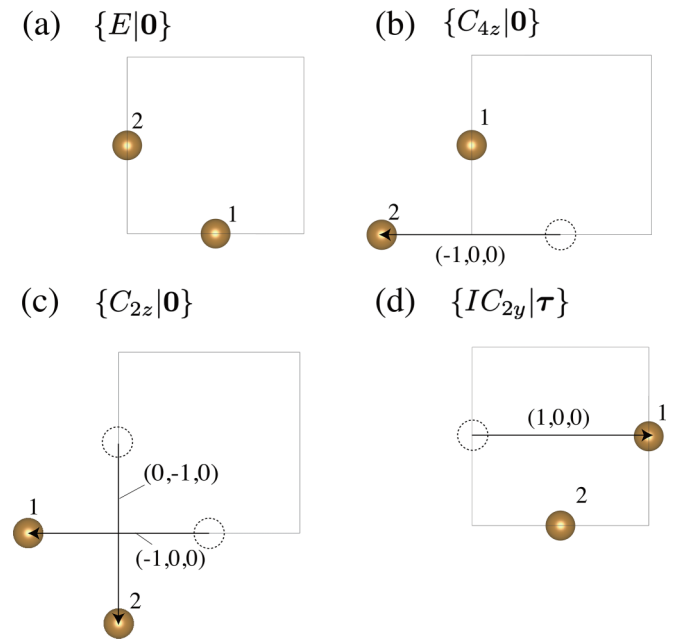


FIG. 3. Transformation properties of atoms on  $2b$  site in a crystallographic system with space group  $P4bm$ . The arrow represents primitive translation vector  $\mathbf{R}_{i_\zeta}^\alpha$  associated with each space group operator (see main text).



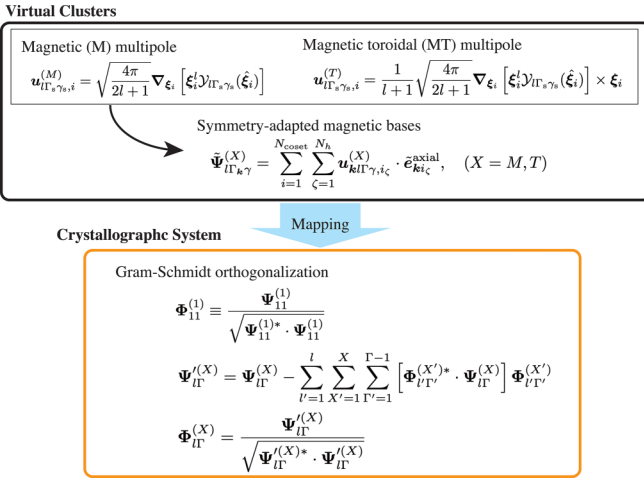


FIG. 4. Outline of magnetic bases generation.

$$\Psi_{l\Gamma}^{(X)} = \Psi_{l\Gamma}^{(X)} - \sum_{\Gamma'=1}^l \sum_{X'=1}^X \sum_{\Gamma''=1}^{\Gamma-1} [\Phi_{l\Gamma''}^{(X')*} \cdot \Psi_{l\Gamma}^{(X)}] \Phi_{l\Gamma''}^{(X')}, \quad (17)$$

$$\Phi_{l\Gamma}^{(X)} = \frac{\Psi_{l\Gamma}^{(X)}}{\sqrt{\Psi_{l\Gamma}^{(X)*} \cdot \Psi_{l\Gamma}^{(X)}}}, \quad (18)$$

where  $\Phi_{l\Gamma}^{(X)}$  is the orthonormal magnetic basis and we reexpress types of multipoles with  $X = M$  and  $T$  by the numbers  $X = 1$  and  $2$ , respectively, and abbreviate the IRREP of  $\mathbf{k}$ -group  $\Gamma_{\mathbf{k}}$  and its component  $\gamma$  by  $\Gamma$ . The magnetic bases generation procedure is summarized in Fig. 4. Although resultant magnetic bases are generally complex, we can always construct real (physical) magnetic bases by taking linear combinations of bases with  $\mathbf{k}$  and  $-\mathbf{k}$ . The present method can be applied to incommensurate magnetic structures. In numerical calculations, it may be treated by approximating the magnetic structure to a commensurate magnetic structure over a long period.

#### D. Multiple- $\mathbf{k}$ states

A single- $\mathbf{k}$  magnetic structure with propagation vector  $\mathbf{k}$  in an IRREP  $\Gamma_{\mathbf{k}}$  of  $\mathbf{k}$ -group  $\mathcal{G}_{\mathbf{k}}$  is a basis vector in an IRREP of  $\mathcal{G}$ , that is  $(\Gamma_{\mathbf{k}} \uparrow \mathcal{G}) \downarrow \mathcal{G}_{\mathbf{k}} = \Gamma_{\mathbf{k}}$  [11,24]. Multiple- $\mathbf{k}$  magnetic structures are induced as bases of IRREPs in space group  $\mathcal{G}$  from single- $\mathbf{k}$  magnetic structure bases with IRREPs in  $\mathcal{G}_{\mathbf{k}}$  by taking account of the following relation between  $\mathcal{G}_{\mathbf{k}}$  and  $\mathcal{G}$  [11,24]:

$$\mathcal{G} = \sum_{i=1}^{S_{\mathbf{k}}} \{p_i | \tau_i\} \mathcal{G}_{\mathbf{k}}, \quad (19)$$

where  $\{p_1 | \tau_1\} = \{E | \mathbf{0}\}$  and  $\{p_i | \tau_i\}$  for  $i \geq 2$  is the symmetry operation of space group  $\mathcal{G}$  not included in  $\mathbf{k}$ -group  $\mathcal{G}_{\mathbf{k}}$ . The set of wave vectors  $\mathbf{k}_i \equiv p_i \mathbf{k}$  ( $i = 1, 2, \dots, S_{\mathbf{k}}$ ) which are inequivalent with each other are called the star of  $\mathbf{k}$ . The bases in IRREP of  $\mathcal{G}$  having propagation vector  $\mathbf{k}_i$  can be generated by acting  $\{p_i | \tau_i\}$  on a single- $\mathbf{k}$  magnetic structure with IRREP  $\Gamma_{\mathbf{k}}$  of  $\mathcal{G}_{\mathbf{k}}$ . Dimension of IRREPs of  $\mathcal{G}$  is therefore equal to that of  $\mathcal{G}_{\mathbf{k}}$  multiplied by  $S_{\mathbf{k}}$ . The multiple- $\mathbf{k}$  magnetic

structures formed as linear combination of the symmetry-adapted single- $\mathbf{k}$  structures with propagation vectors associated with each other by symmetry operations  $\{p_i | \tau_i\}$  in Eq. (19) can preserve the higher rotational symmetry than that of the single- $\mathbf{k}$  structures, while it makes the translational symmetry lower than that under the single- $\mathbf{k}$  structures.

To gain a clear insight into multiple- $\mathbf{k}$  magnetic states constructed from single- $\mathbf{k}$  states, we here discuss two pedagogical examples of multiple- $\mathbf{k}$  states: double- $\mathbf{k}$  states on the square lattice and triple- $\mathbf{k}$  states on the face centered cubic (FCC) structure. Note that the former is one of the simplest examples of multiple- $\mathbf{k}$  magnetic structures, which is appropriate for an intuitive understanding of multiple- $\mathbf{k}$  magnetic structures. Indeed, several real compounds with the FCC structure are known to exhibit multiple- $\mathbf{k}$  magnetic orderings. A nonsymmorphic example will be discussed later in Sec. III B.

The double- $\mathbf{k}$  states having high magnetic point group symmetry with propagation vectors  $\mathbf{k} = (\frac{1}{2}, 0, 0)$  and  $(0, \frac{1}{2}, 0)$  on the square lattice as well as the single- $\mathbf{k}$  states are shown in Fig. 5. The double  $\mathbf{k}$  states are obtained as linear combinations of single- $\mathbf{k}$  states  $\psi_1$  and  $\psi_2$  as shown in Fig. 5. Note that the space group of the square lattice is  $P4/mmm$  and point group preserving  $\mathbf{k}$ , referred as  $\mathbf{k}$ -point group, is  $D_{2h}$ . In this case, all IRREPs of  $\mathcal{G}_{\mathbf{k}}$  are one-dimensional and  $S_{\mathbf{k}} = 2$ , leading to two-dimensional IRREPs under  $\mathcal{G}$ . The representation matrices for several space group elements are also explicitly shown in Fig. 5. We can see that in the single- $\mathbf{k}$  (double- $\mathbf{k}$ ) states, the representation matrix for translational symmetry  $\{E | \mathbf{R}_a\}$  with  $\mathbf{R}_a = (1, 0, 0)$  has diagonal (nondiagonal) form, while that for rotational operation  $\{C_{4z} | \mathbf{0}\}$  or  $\{C_{4z} | \mathbf{R}_a\}$  has nondiagonal (diagonal) form. This indicates that the rotational symmetry in double- $\mathbf{k}$  states is higher than that in the single- $\mathbf{k}$  states but translational symmetry in the double- $\mathbf{k}$  states is lower than that in the single- $\mathbf{k}$  states, as mentioned before. It should be noted that time-reversal symmetry is retained macroscopically both in the single- and double- $\mathbf{k}$  states, that is, the time-reversal operation combined with translational operation is preserved in the magnetic states. As a result, the magnetic point group in the double- $\mathbf{k}$  states shown in Fig. 5 is same as in the paramagnetic state, that is  $4/mmm1'$ , whereas that in the single- $\mathbf{k}$  states is orthorhombic one  $mmm1'$ , which is lower than  $4/mmm1'$ . The breaking of four fold rotational symmetry along  $z$  axis in the single- $\mathbf{k}$  states is understood from the uniaxial folding of the Brillouin zone along  $x$  or  $y$  direction from the paramagnetic state to magnetic state. This type of magnetic ordering causing breaking of four fold rotational symmetry has been discussed in the context of iron-pnictides [26,27].

The examples of triple- $\mathbf{k}$  states with propagation vectors at the  $X$  points,  $\mathbf{k}_1 = (1, 0, 0)$ ,  $\mathbf{k}_2 = (0, 1, 0)$ , and  $\mathbf{k}_3 = (0, 0, 1)$ , on FCC lattice are also shown in Figs. 6(a) and 6(b). The space group of FCC lattice is  $Fm\bar{3}m$  and the  $\mathbf{k}$ -point group is  $D_{4h}$ . Note that the magnetic structure in Fig. 6(a) has been observed in Fe-Mn alloys [28–30] and several  $f$ -electron compounds such as NpX ( $X = \text{As, Sb, Bi}$ ) [31–34] and U5B [34–36]. In contrast to the square lattice discussed above, there are two types of two-dimensional IRREPs,  $E_g^-$  and  $E_u^-$ -IRREPs, in addition to the eight types of one-dimensional IRREPs of  $D_{4h}$   $\mathbf{k}$ -point group at the  $X$  points. Here and hereafter, we label the odd (even) parity for time-reversal

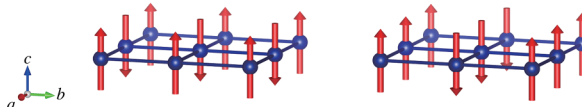
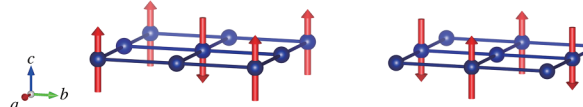
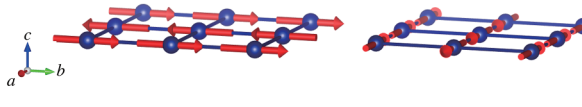
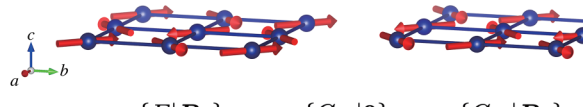
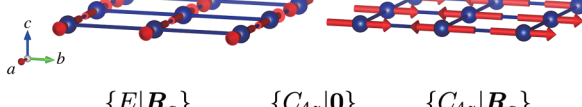
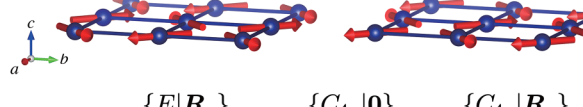
	single- $\mathbf{k}$	double- $\mathbf{k}$
$B_{1g}^-$	(a) $\psi_1$ $\psi_2$  $\{E \mathbf{R}_a\}$ $\{C_{4z} \mathbf{0}\}$ $\{C_{4z} \mathbf{R}_a\}$ $\begin{pmatrix} -1 & 0 \\ 0 & 1 \end{pmatrix}$ $\begin{pmatrix} 0 & 1 \\ 1 & 0 \end{pmatrix}$ $\begin{pmatrix} 0 & -1 \\ 1 & 0 \end{pmatrix}$	(b) $\psi_1 + \psi_2$ $\psi_1 - \psi_2$  $\{E \mathbf{R}_a\}$ $\{C_{4z} \mathbf{0}\}$ $\{C_{4z} \mathbf{R}_a\}$ $\begin{pmatrix} 0 & -1 \\ -1 & 0 \end{pmatrix}$ $\begin{pmatrix} 1 & 0 \\ 0 & -1 \end{pmatrix}$ $\begin{pmatrix} 0 & 1 \\ -1 & 0 \end{pmatrix}$
$B_{2g}^-$	(c) $\psi_1$ $\psi_2$  $\{E \mathbf{R}_a\}$ $\{C_{4z} \mathbf{0}\}$ $\{C_{4z} \mathbf{R}_a\}$ $\begin{pmatrix} -1 & 0 \\ 0 & 1 \end{pmatrix}$ $\begin{pmatrix} 0 & -1 \\ 1 & 0 \end{pmatrix}$ $\begin{pmatrix} 0 & 1 \\ 1 & 0 \end{pmatrix}$	(d) $\psi_1 + \psi_2$ $\psi_1 - \psi_2$  $\{E \mathbf{R}_a\}$ $\{C_{4z} \mathbf{0}\}$ $\{C_{4z} \mathbf{R}_a\}$ $\begin{pmatrix} 0 & -1 \\ -1 & 0 \end{pmatrix}$ $\begin{pmatrix} 0 & 1 \\ -1 & 0 \end{pmatrix}$ $\begin{pmatrix} 1 & 0 \\ 0 & -1 \end{pmatrix}$
$B_{3g}^-$	(e) $\psi_1$ $\psi_2$  $\{E \mathbf{R}_a\}$ $\{C_{4z} \mathbf{0}\}$ $\{C_{4z} \mathbf{R}_a\}$ $\begin{pmatrix} -1 & 0 \\ 0 & 1 \end{pmatrix}$ $\begin{pmatrix} 0 & -1 \\ 1 & 0 \end{pmatrix}$ $\begin{pmatrix} 0 & 1 \\ 1 & 0 \end{pmatrix}$	(f) $\psi_1 + \psi_2$ $\psi_1 - \psi_2$  $\{E \mathbf{R}_a\}$ $\{C_{4z} \mathbf{0}\}$ $\{C_{4z} \mathbf{R}_a\}$ $\begin{pmatrix} 0 & -1 \\ -1 & 0 \end{pmatrix}$ $\begin{pmatrix} 0 & 1 \\ -1 & 0 \end{pmatrix}$ $\begin{pmatrix} 1 & 0 \\ 0 & -1 \end{pmatrix}$

FIG. 5. [(a), (c), and (e)] Single- $\mathbf{k}$  and [(b), (d), and (f)] double- $\mathbf{k}$  magnetic structures with  $\mathbf{k} = (\frac{1}{2}, 0, 0)$  and  $(0, \frac{1}{2}, 0)$  on the square lattice. The representation matrices for symmetry operations  $\{E|\mathbf{0}\}$ ,  $\{C_{4z}|\mathbf{0}\}$ , and  $\{C_{4z}|\mathbf{R}_a\}$  with  $\mathbf{R}_a = (1, 0, 0)$  are also shown.

symmetry as superscript  $-$  ( $+$ ) in IRREPs such as  $E_g^-$  ( $E_g^+$ ). The two- and one-dimensional IRREPs under  $\mathcal{G}_k$  with  $S_k = 3$  form six- and three-dimensional IRREPs under  $\mathcal{G}$  since the  $X$  points  $(1,0,0)$ ,  $(0,1,0)$ , and  $(0,0,1)$  are transformed into each other by symmetry operations  $\{E|\mathbf{0}\}$ ,  $\{C_{3[111]}|\mathbf{0}\}$ , and

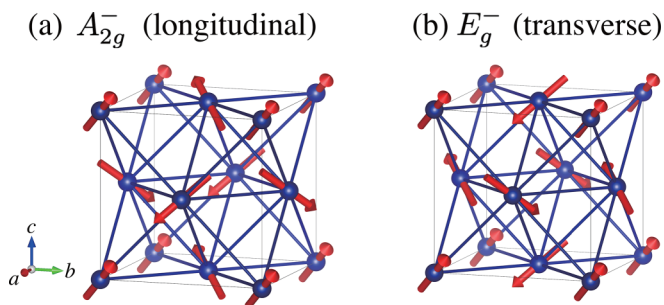


FIG. 6. Triple- $\mathbf{k}$  magnetic structures on the FCC lattice induced from magnetic structures with  $\mathbf{k} = (1, 0, 0)$  having (a)  $A_{2g}^-$  and (b)  $E_g^-$  representations.

$\{C_{3[111]}^2|\mathbf{0}\}$ , where  $C_{3[111]}$  is three fold rotation along  $[111]$  direction. The single- $\mathbf{k}$  magnetic state with propagation vector  $\mathbf{k}_i$  ( $i = 1, 2, 3$ ) preserves macroscopic time-reversal symmetry since  $\mathbf{k}_i$  is a time-reversal invariant momentum. On the contrary, any linear combination of single- $\mathbf{k}$  magnetic bases with  $\mathbf{k}_i$  to form triple- $\mathbf{k}$  states necessarily breaks macroscopic time-reversal symmetry. For instance, when a translational operation  $\mathbf{t}$  carries the factor  $-1$  for the magnetic bases with  $\mathbf{k}_1$  and  $\mathbf{k}_2$ , and then same translation carries factor  $+1$  for that with  $\mathbf{k}_3 = -\mathbf{k}_1 - \mathbf{k}_2$ . Since all the magnetic bases with  $\mathbf{k}_i$  ( $i = 1, 2, 3$ ) cannot be simultaneously transformed into themselves with factor  $-1$  under a primitive translation  $\mathbf{t}$ , the triple- $\mathbf{k}$  magnetic ordering breaks the macroscopic time-reversal symmetry. As a result, the triple- $\mathbf{k}$  magnetic order is accompanied with the secondary uniform magnetic order parameter, that is, magnetic multipoles with  $\mathbf{k} = \mathbf{0}$ . In the present case, triple- $\mathbf{k}$  magnetic ordering induces the secondary uniform magnetic order parameter having  $A_{2g}^-$ -IRREP of  $O_h$  point group. The experimentally observed all-in-all-out type magnetic order in a pyrochlore oxide  $\text{Cd}_2\text{Os}_2\text{O}_7$  with space

group  $Fd\bar{3}m$  [37] has the same symmetry of the secondary magnetic order parameter,  $A_{2g}^-$ , of the triple- $\mathbf{k}$  state in the FCC lattice, as shown in Fig. 6(a). Arima has pointed out that the all-in-all-out magnetic order can be regarded as a ferroic order of magnetic octupole  $M_{xyz}$  and leads to several intriguing phenomena such as asymmetric magnetization and linear magnetostriction [38]. It is, therefore, expected that similar phenomena emerge also in Fe-Mn alloys, NpX, and USb. On the other hand, the triple- $\mathbf{k}$  state shown in Fig. 6(b) is induced from the magnetic structure with  $E_g^-$ -symmetry of  $\mathbf{k}$  group at X point. This type of magnetic ordering has been observed in  $\text{UO}_2$  [39–42]. This magnetic ordering with magnetic point group  $m\bar{3}$  is absence of anti-unitary symmetry operations, which belongs to type-I Shubnikov group [11]. The absence of anti-unitary symmetry operations indicates that the axial (polar) tensors having opposite parities for time-reversal operation, that is, M (MT) and ET (E) multipoles cannot be distinguished from the symmetry viewpoint. These multipoles thus are simultaneously activated in this situation [43], resulting in intriguing physical phenomena. For instance, the electric toroidal dipolar moment as well as the magnetic moment are linearly coupled with magnetic field in the magnetic state shown in Fig. 6(b). The crystal symmetry is thus lowered to  $C_{2h}$  by magnetic field along [001] axis in contrast to the case of similar paramagnetic point group  $m\bar{3}1'$ , in which the crystal symmetry is lowered to  $D_{2h}$  by magnetic field along [001] axis. Such characteristic magnetostriction is useful for identifying the order parameter.

### III. APPLICATION TO REPRESENTATIVE AHE ANTIFERROMAGNETS

#### A. $\alpha$ -Mn

Unary manganese forms various crystal structures depending on temperature, which are called  $\alpha$ -,  $\beta$ -,  $\gamma$ -, and  $\delta$ -Mn [44].  $\alpha$ -Mn with body centered cubic (BCC) structure, which is realized at  $T \lesssim 980$  K, has attracted interest due to its intriguing and complex magnetic properties. A noncollinear antiferromagnetism with ordering vector  $\mathbf{k} = \mathbf{k}_H \equiv (1, 0, 0)$  is realized at  $T \lesssim 95$  K [45–49] under an ambient pressure, while a first-order transition to the another magnetic phase with tiny net magnetization  $\sim 0.02 \mu_B/\text{Mn}$  takes place under an applied pressure  $P \sim 1.4$  GPa [50–52]. The recent experimental study has revealed the emergence of large anomalous Hall response reaching  $\sigma_{xy} \sim 400\text{--}600 \text{ S cm}^{-1}$  in the high-pressure phase despite such small net magnetization [51]. We here apply our theory to  $\alpha$ -Mn to generate magnetic structures at high-symmetry  $\mathbf{k}$  points and provide a possible scenario for large anomalous Hall response in the high-pressure magnetic phase, in which magnetic structure has not been clarified experimentally.

Figure 7 shows the crystal structure and the corresponding first Brillouin zone for  $\alpha$ -Mn. The primitive (conventional) unit cell contains 29 (58) Mn atoms and resulting crystal structure is relatively complicated. The space group symmetry of  $\alpha$ -Mn is  $I43m$  (No. 217,  $T_d^3$ ), and there are four distinct types of Mn-sites, Mn-I, Mn-II, Mn-III, and Mn-IV sites which are located on 2a, 8c, 24g, and 24g Wyckoff positions, respectively. The sizes of local magnetic moments largely

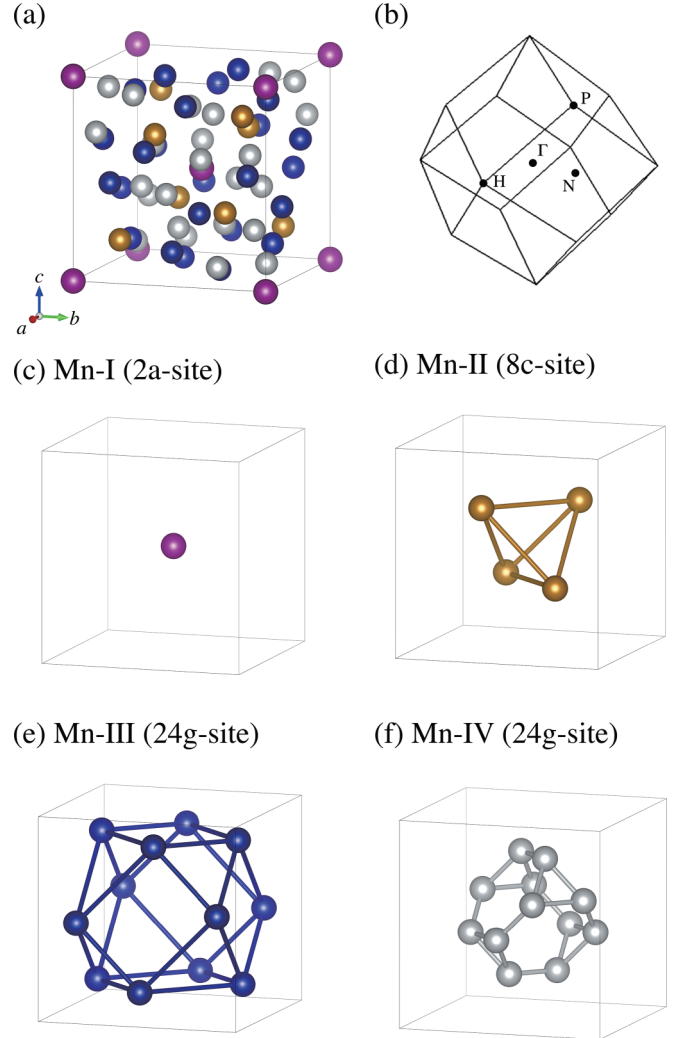


FIG. 7. (a) Crystal structure and (b) first Brillouin zone of  $\alpha$ -Mn. Mn-I, -II, -III, and -IV sites are separately shown in (c), (d), (e), and (f), respectively, where body-centered sites are not shown.

depend on the types of Mn-sites according to experiments in the AFM phase at ambient pressure. The magnetic moments on Mn-I and -II sites are quite larger than those on Mn-III and -IV sites, as shown in Table III [47–49] and a similar tendency for local magnetic moments is obtained by the first-principles calculations [53–56]. In addition, the internal magnetic fields on Mn-III and -IV sites are rapidly suppressed by an applied pressure according to the recent zero-field NMR

TABLE III. Local magnetic moments in units of  $\mu_B$  on each Mn site in AFM phase in  $\alpha$ -Mn at ambient pressure from Ref. [49]. Note that Mn-III and Mn-IV sites are split into two different types of Mn sites due to lacking of  $C_3$  symmetry in AFM phase.

	I	II	III-1	III-2	IV-1	IV-2
$m_x$	0.0	0.14	0.43	-0.25	0.27	-0.08
$m_y$	0.0	0.14	0.43	-0.25	0.27	-0.45
$m_z$	2.83	1.82	0.43	-0.32	-0.45	-0.48
$ \mathbf{m} $	2.83	1.83	0.74	0.48	0.59	0.66

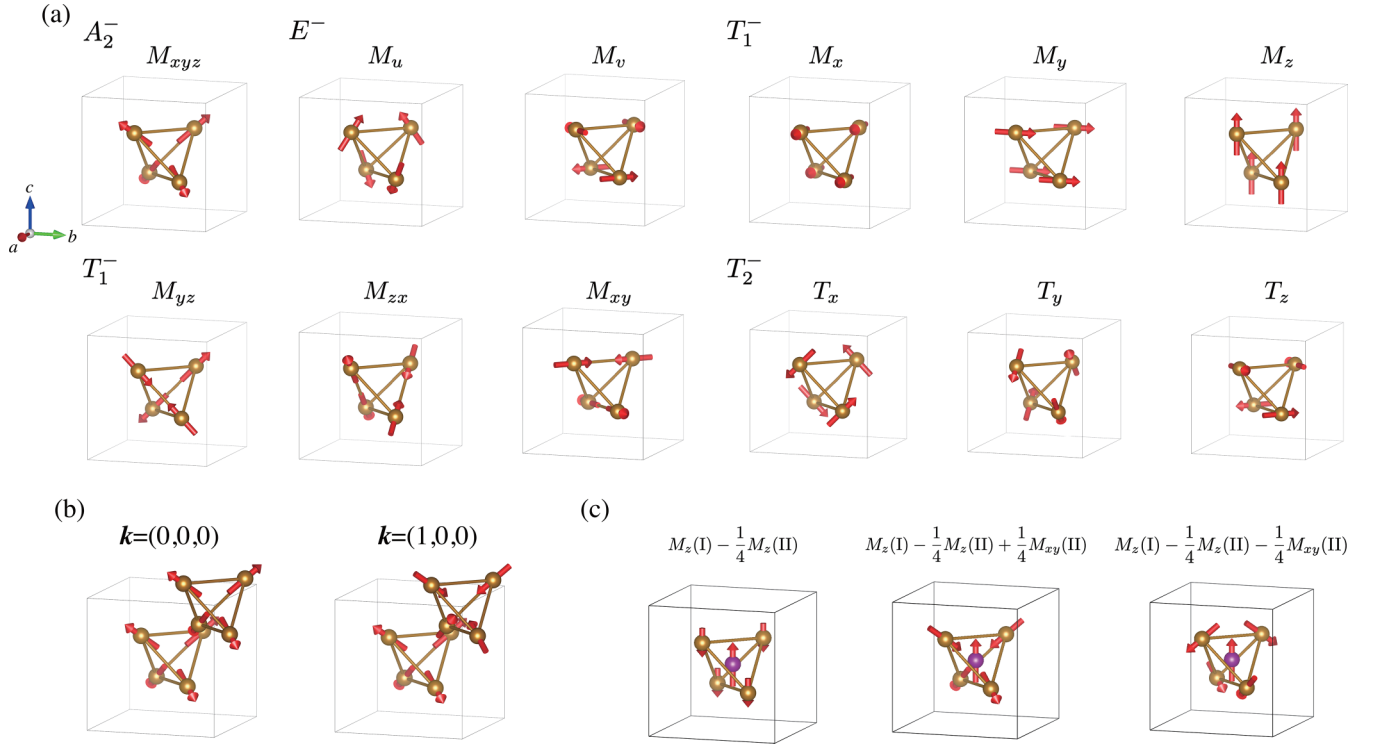


FIG. 8. (a) Magnetic structure bases with  $\mathbf{k} = \mathbf{0}$  on Mn-II sites in  $\alpha$ -Mn. (b) Comparison between magnetic basis having  $A_2^-$ -IRREP with  $\mathbf{k} = \mathbf{0}$  and that with  $\mathbf{k} = (1, 0, 0)$ . (c) Examples of magnetic structures without net magnetization compatible with finite AHE  $\sigma_{xy} \neq 0$ .

measurements [57]. We thus focus on magnetic structures on Mn-I and -II sites in this paper.

Nonzero anomalous Hall response requires symmetry breaking same as ferromagnetic ordering, which belongs to  $T_1^-$ -IRREP with  $\mathbf{k} = \mathbf{0}$  under  $T_d$ -point group in the present system [1,22,43,58–60]. According to the recent neutron diffraction measurements, the magnetic reflection observed in the ambient pressure phase is absent in the high-pressure phase [61]. Therefore we focus on the cases of magnetic orderings having  $T_1^-$  symmetry with ordering vector  $\mathbf{k} = \mathbf{0}$  and  $\mathbf{k} = \mathbf{k}_H = (1, 0, 0)$  in the present study.

The transformation properties for arbitrary magnetic structures on each Wyckoff position are encoded in representation matrices, which are called magnetic representations. The magnetic representations of  $2a$  and  $8c$  sites,  $D_{2a}^{(\text{mag})}$  and  $D_{8c}^{(\text{mag})}$ , are decomposed into IRREPs of  $\mathcal{G}_k$  with  $\mathbf{k} = \mathbf{0}$  as follows:

$$D_{2a}^{(\text{mag})} = T_1^-, \quad (20)$$

$$D_{8c}^{(\text{mag})} = A_2^- \oplus E^- \oplus 2T_1^- \oplus T_2^-, \quad (21)$$

where we use Mulliken notation for IRREPs under  $T_d$  point group since IRREPs of  $\mathcal{G}_k$  with  $\mathbf{k} = \mathbf{0}$  are equivalent to those of crystallographic point group of  $\mathcal{G}$ . We show the symmetry-adapted magnetic structures at  $8c$  site with  $\mathbf{k} = \mathbf{0}$  in Fig. 8(a), which are similar to the magnetic structures on pyrochlore structures [62,63]. Note that the magnetic structures having  $\mathbf{k} = \mathbf{k}_H$  can be obtained by reversing magnetic moments on body center tetrahedra for those with  $\mathbf{k} = \mathbf{0}$  as shown in Fig. 8(b). The obtained magnetic structure bases with  $\mathbf{k} = \mathbf{k}_H$  are consistent with the preceding group theoretical analysis of neutron diffraction experiment [46].

From Eqs. (20) and (21) and Fig. 8(a), we can see that there are two sets of magnetic structure bases on  $8c$  site with  $T_1^-$ -IRREP whereas there is one set of magnetic structures on  $2a$  site with  $T_1^-$ -IRREP, that is, ferromagnetic structure. One of  $T_1^-$ -IRREP magnetic structures on  $8c$  site corresponds to the ordinary ferromagnetism, and the other is noncollinear antiferromagnetism without net magnetization. The linear combinations of these magnetic bases can generate nonzero anomalous Hall response  $\sigma_{xy} \neq 0$ . The magnetic structures without net magnetization are shown in Fig. 8(c). It is noteworthy that odd parity M and MT multipoles such as the M quadrupole ( $M_{yz}, M_{zx}, M_{xy}$ ) and MT octupole ( $T_x^\beta, T_y^\beta, T_z^\beta$ ) belong to the same  $T_1^-$ -IRREP of the primary order parameter under the point group  $T_d$ . These thus can be finite in magnetic structures with nonzero AHE. Since the odd-parity MT multipoles are closely related to the second-order electrical conductivity tensor  $\sigma_{i,jk}$  [43,64–69], the nonlinear charge transport can emerge in the high-pressure magnetic phase of  $\alpha$ -Mn [70]. The off-diagonal components  $\sigma_{xzx}, \sigma_{yyz}, \sigma_{zxx}$ , and  $\sigma_{zyy}$  are finite while the other components including diagonal ones  $\sigma_{i,ii}$  vanish in the present case. This form of the tensor  $\sigma_{i,jk}$  indicates that both the longitudinal and transverse currents can be generated under an applied electric field except for several specific cases.

We here discuss the secondary order parameters based on the Landau theory [71,72], which gives clear insight into physical phenomena in the ordered phases and useful information about primary order parameters. In fact, detailed analysis for couplings between primary and secondary order parameters leads to deep understanding of complex multipolar ordered phases in the  $f$ -electron systems [20,73–76].



The possible secondary order parameters are characterized by  $\mathbf{k} = \mathbf{0}$  in case the primary order parameter has the ordering vector  $\mathbf{k} = \mathbf{0}$ . We first discuss the electric degrees of freedom induced by the magnetic orderings, which are relevant to elastic response and Edelstein effect, for instance. The electric order parameters, which are time-reversal-even, are induced by the coupling of the electric multipoles to the even order terms of magnetic ones in Landau free energy expression due to the time-reversal symmetry in the paramagnetic phase. The electric order parameters emerging through the lowest third-order terms, can be deduced by irreducible decomposition of symmetric product of primary order parameters as follows:

$$[T_1^- \otimes T_1^-] = A_1^+ \oplus E^+ \oplus T_2^+, \quad (22)$$

where the secondary order parameters with  $A_1^+$ ,  $E^+$ , and  $T_2^+$ -IRREPs correspond to uniform electric monopole  $Q_0$ , electric quadrupoles ( $Q_{u(=3z^2-r^2)}$ ,  $Q_{v(=x^2-y^2)}$ ), and ( $Q_{yz}$ ,  $Q_{zx}$ ,  $Q_{xy}$ ), respectively from the symmetry viewpoint. Note that in the present case, electric toroidal quadrupole (electric dipole) ( $G_v$ ,  $G_u$ ) [ $(Q_x, Q_y, Q_z)$ ] also emerges when electric quadrupole ( $Q_u, Q_v$ ) [ $(Q_{yz}, Q_{zx}, Q_{xy})$ ] is finite since those have the same IRREP  $E^+$  ( $T_2^+$ ) under  $T_d$  point group. The explicit forms of the third-order terms in Landau free energy are given as follows:

$$\begin{aligned} F^{(3)} = & c_1 [M_y M_z Q_{yz} + (\text{cyclic perm.})] \\ & + c_2 \sqrt{3} (M_x^2 - M_y^2) Q_v \\ & + c_2 (2M_z^2 - M_x^2 - M_y^2) Q_u, \end{aligned} \quad (23)$$

where we neglect trivial coupling with the fully symmetric  $Q_0$  term and (cyclic perm.) represents the terms obtained by cyclic permutations for indices of  $M_y M_z Q_{yz}$  as  $x, y, z \rightarrow y, z, x$  and  $z, x, y$ , and  $c_1$  and  $c_2$  are coupling constants determined from microscopic models. Equation (23) represents that the electric quadrupole is inevitably induced by primary order parameter with  $T_1^-$ -IRREP. For example,  $Q_u$ -type electric quadrupole emerges in the case that  $M_x = M_y = 0$  and  $M_z \neq 0$  while the electric quadrupoles having  $T_2^+$  symmetry emerge with the same amplitude of all components, that is,  $Q_{yz} = Q_{zx} = Q_{xy} \neq 0$  in the case that  $M_x = M_y = M_z \neq 0$ . Therefore the symmetry of crystal structure is lowered to tetragonal  $D_{2d}$  point group in the former case, which can induce gyrotropic magnetic effect, and polar trigonal  $C_{3v}$  point group in the latter case. Note that similar couplings to electric multipoles with  $\mathbf{k} = \mathbf{0}$  emerges also in the case of the primary order parameter with  $\mathbf{k} = \mathbf{k}_H$  since the even powers of primary order parameters carry the wave vector  $\mathbf{k} = \mathbf{0}$  modulo reciprocal lattice vector.

In the similar manner, secondary magnetic order parameters are discussed. Due to the time reversal symmetry in the nonmagnetic phase, the secondary magnetic order parameter emerges through the fourth-order coupling in the Landau free energy, which can be obtained by the irreducible decomposition of fully symmetric product  $[T_1^- \otimes T_1^- \otimes T_1^-]$  as follows:

$$[T_1^- \otimes T_1^- \otimes T_1^-] = A_2^- \oplus 2T_1^- \oplus T_2^-, \quad (24)$$

where  $A_2^-$  and  $T_2^-$  correspond to magnetic octupoles  $M_{xyz}$  and  $(M_x^\beta, M_y^\beta, M_z^\beta)$  from the symmetry viewpoint. The fourth-order term of Landau free energy which represent coupling of order parameter with  $T_1^-$ -IRREP to the secondary order parameters having different symmetry is given as follows:

$$\begin{aligned} F^{(4)} = & d_1 M_x M_y M_z M_{xyz} \\ & + d_2 [(M_y^2 - M_z^2) M_x M_x^\beta + (\text{cyclic perm.})]. \end{aligned} \quad (25)$$

From the above equation, we can see that in the case of  $M_x = M_y = 0$  and  $M_z \neq 0$ , the magnetic secondary order parameter does not emerge while in the case of  $M_x = M_y = M_z \neq 0$  ( $M_z = 0$  and  $M_x = M_y \neq 0$ ), the magnetic octupole  $M_{xyz}$  ( $M_x^\beta = -M_y^\beta$ ) is induced. On the other hand, when the primary order parameter has a modulation vector  $\mathbf{k} = \mathbf{k}_H$ , secondary magnetic order parameters with  $\mathbf{k} = \mathbf{0}$  do not emerge since combined symmetry of time-reversal operation and primitive translation retains in the ordered phase. The secondary induced magnetic multipoles have ordering vector  $\mathbf{k} = \mathbf{k}_H$  in this case.

The primary order parameters with inducing the secondary order parameters discussed above give rise to deformation of electronic states and resulting physical phenomena in the ordered phases. In particular, the order parameters with the ordering vector  $\mathbf{k} = \mathbf{0}$  are important since those can be sources of macroscopic responses according to Neumann's principle [22,58,60,77] and experiments using macroscopic probes can detect the order parameters relatively easier. The magnetic order parameter  $M_z$  with  $\mathbf{k} = \mathbf{0}$  is finite in the high-pressure phase, while that vanishes in the ambient pressure phase. The former case leads to anomalous Hall, Nernst effects, and magneto-optical effects.

On the other hand, electric order parameters  $Q_u$  and  $G_v$  with  $\mathbf{k} = \mathbf{0}$  can be finite in both ambient and high-pressure magnetic phases. This gives rise to the antisymmetric spin-splitting of band structures  $k_x \sigma_x - k_y \sigma_y$ , resulting in natural optical activity and magnetocurrent effect such as the Edelstein effect [78–80], where  $\sigma_i$  ( $i = x, y, z$ ) is the Pauli spin matrix. We summarize band deformations as the hopping terms in the  $2 \times 2$  Hamiltonian with spin degree of freedom and macroscopic responses in the ordered phases in Table IV.

TABLE IV. Band deformation and macroscopic responses in the magnetic ordered phases having  $T_1^-$ -IRREP with the ordering vectors  $\mathbf{k} = \mathbf{0}$  ( $\Gamma$  point) in the high-pressure phase and  $\mathbf{k} = \mathbf{k}_H$  (H point) in the ambient pressure phase. AHE, ANE, ME, MC, and MOKE represent anomalous Hall, anomalous Nernst, magnetoelectric, magnetocurrent, and magneto-optical Kerr effects, respectively and NLC denotes the nonlinear charge transport. Note that magneto-current effects correspond to Edelstein effect and its inverse response.

ordering vector	band deformation			macroscopic response
$\Gamma : (0, 0, 0)$	$(3k_z^2 - k^2)\sigma_0$	$k_x \sigma_x - k_y \sigma_y$	$\sigma_z$	$k_z(k_x^2 - k_y^2)\sigma_0$
$H : (1, 0, 0)$	$(3k_z^2 - k^2)\sigma_0$	$k_x \sigma_x - k_y \sigma_y$	$\boldsymbol{\chi}$	$\boldsymbol{\chi}$
				AHE, ANE, MOKE, ME, MC, NLC MC

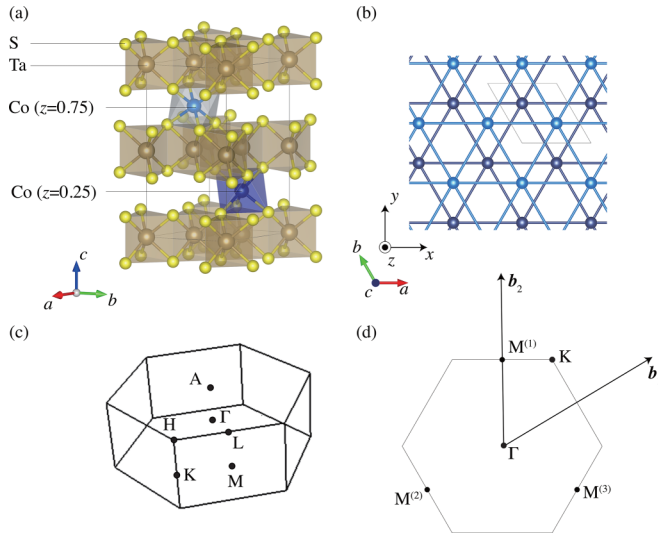


FIG. 9. (a) Crystal structure of  $\text{CoTa}_3\text{S}_6$  and (b) that on  $ab$  plane with only Co atoms. (c) First Brillouin zone for  $\text{CoTa}_3\text{S}_6$  and (d) that on  $k_z = 0$  plane, where several high-symmetry  $\mathbf{k}$  points are shown by dots.

### B. $\text{CoM}_3\text{S}_6$

An intercalated compound of transition metal dichalcogenides,  $\text{TM}_3\text{S}_6$  ( $T = 3d$ -transition metal,  $M = \text{Nb}, \text{Ta}$ ), shows rich electronic and magnetic properties. For instance, a helimagnetic ordering with a long period is formed in  $\text{CrNb}_3\text{S}_6$  [81,82], which turns into chiral soliton lattice under an applied magnetic field. Another compound, ferromagnetic  $\text{VM}_3\text{S}_6$  is proposed as a candidate of Weyl semimetals or topological insulators by first-principles calculations [83].  $\text{CoNb}_3\text{S}_6$  in particular has attracted growing interests due to its large anomalous Hall conductivity in the magnetic ordered phase with a tiny ferromagnetic moment [84–86]. This compound crystallizes in the space group  $P6_322$  (No. 182,  $D_6^2$ ) symmetry, where the crystal structure is shown in Fig. 9. Early neutron diffraction studies by Parkin *et al.* indicate the magnetic structure with a single- $\mathbf{k}$   $(0, \frac{1}{2}, 0)$  having multidomain for  $\text{CoNb}_3\text{S}_6$  and that with  $\mathbf{k} = (\frac{1}{3}, \frac{1}{3}, 0)$  for  $\text{CoTa}_3\text{S}_6$  [87]. Recent neutron diffraction patterns for  $\text{CoNb}_3\text{S}_6$ , however, are also compatible with multi- $\mathbf{k}$  magnetic order with single domain [85]. We here discuss possible magnetic structures with ordering vector  $\mathbf{k}$  at high-symmetry points in BZ and provide a symmetry analysis of magnetic structures in connection with emergence of anomalous Hall effect.

Let us consider magnetic structures with ordering vectors  $\mathbf{k}$  at  $M$  points. There are three symmetry equivalent  $M$  points in the first Brillouin zone, which are given by  $\mathbf{k}_{M^{(1)}} = (0, \frac{1}{2}, 0)$ ,  $\mathbf{k}_{M^{(2)}} = (-\frac{1}{2}, 0, 0)$ , and  $\mathbf{k}_{M^{(3)}} = (\frac{1}{2}, -\frac{1}{2}, 0)$  as shown in Figs. 9(c) and 9(d). The  $\mathbf{k}$ -point group at  $M$  points is  $D_2$  and magnetic bases can be classified according to IRREPs under this point group (see Table V). Figure 10 shows symmetry adapted magnetic structures with a single propagation vector  $\mathbf{k} = \mathbf{k}_{M^{(1)}}$ . All the magnetic structures in Fig. 10 are collinear antiferromagnetism. Note that we can construct noncollinear magnetic structures as linear combinations of (b) and (e) and those of (d) and (f) without further symmetry lowering since the magnetic structures in Figs. 10(b) and 10(e) and those in

TABLE V. Character table for  $\mathbf{k}$  group at  $M^{(i)}$  point.  $C_{2x,1}$  and  $C_{2y,1}$  represent twofold rotation along  $x$  and  $y$  axes.  $C_{2x(y),i}$  ( $i = 2, 3$ ) is defined as  $C_{2x(y),i} = C_{3z}^{i-1} C_{2x(y),1} C_{3z}^{-i+1}$ .

	$E$	$C_{2z}$	$C_{2y,i}$	$C_{2x,i}$
$A$	1	1	1	1
$B_1$	1	1	-1	-1
$B_2$	1	-1	1	-1
$B_3$	1	-1	-1	1

10(d) and 10(f) have same IRREPs. Symmetry operation of time-reversal combined with primitive lattice translation holds in the magnetic states characterized by  $\mathbf{k} = (0, \frac{1}{2}, 0)$  shown in Fig. 10. As a result, anomalous Hall response is prohibited in these magnetic states.

As mentioned in Sec. II C, triple- $\mathbf{k}$  magnetic structures are obtained from single- $\mathbf{k}$  magnetic bases. Possible high-symmetry triple- $\mathbf{k}$  magnetic structures related to anomalous Hall effect are shown in Figs. 11 and 12. The two magnetic structures, i.e., vortex-like arrangement of magnetic moments

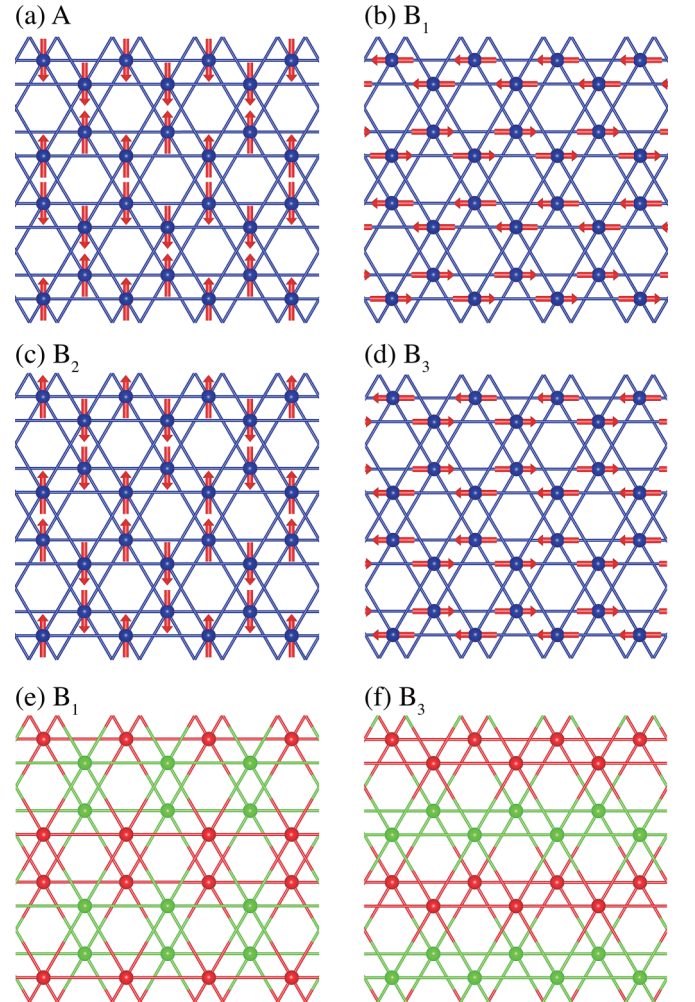


FIG. 10. Magnetic structure bases with single- $\mathbf{k}$   $(0, \frac{1}{2}, 0)$  in crystal structure of  $\text{CoM}_3\text{S}_6$ . The arrow and red (green) sphere represents magnetic moment in  $ab$  plane and along  $+z$  ( $-z$ ) axis, respectively.

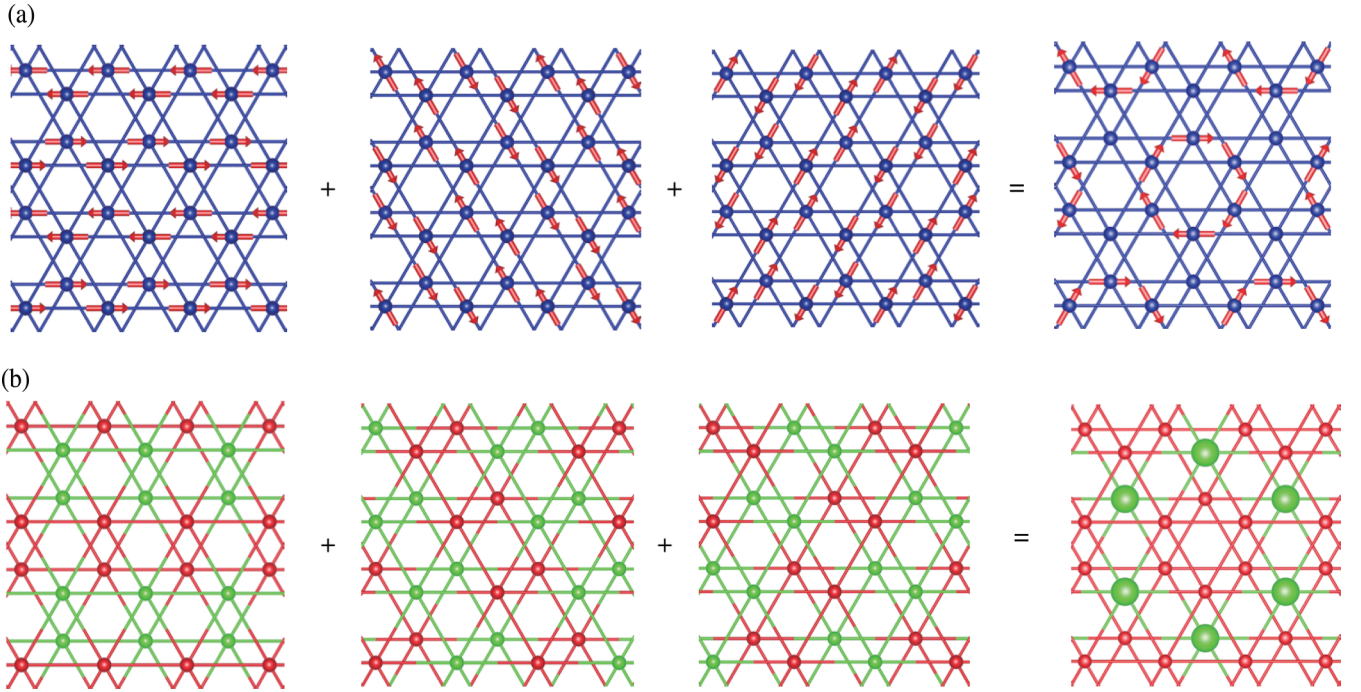


FIG. 11. Triple- $\mathbf{k}$  magnetic structures induced from single- $\mathbf{k}$  magnetic bases with  $B_1^-$  symmetry at  $M$  points. (a) and (b) correspond to those from magnetic bases shown in Figs. 10(b) and 10(e), respectively.

in  $ab$  plane and ferrimagnetic structure along  $c$  axis shown in Fig. 11, can induce AHE since these magnetic point groups are  $62'2'$  [88]. The other high-symmetry triple- $\mathbf{k}$  magnetic states induced from single- $\mathbf{k}$  magnetic states having each of  $A^-$ ,  $B_2^-$ , and  $B_3^-$  symmetry in Table V prohibit AHE since these magnetic point groups are  $622$ ,  $6'2'2$ , and  $6'22'$ , respectively [88]. The Landau free energy expression gives more clear insight into emergence of AHE in magnetically ordered phase. Secondary magnetic order parameters are coupled with the primary ones through the even order terms in the Landau free energy due to time-reversal symmetry in the paramagnetic state. Magnetic multipoles with  $\mathbf{k} = \mathbf{0}$  are coupled with

magnetic order parameters with  $\mathbf{k}_{M^{(i)}}$  through the fourth-order terms in the Landau free energy since the sum of the wave vectors at  $M$  points is zero:  $\mathbf{k}_{M^{(1)}} + \mathbf{k}_{M^{(2)}} + \mathbf{k}_{M^{(3)}} = \mathbf{0}$ . In the case that primary order parameters have  $B_1^-$  symmetry with propagation vector at  $M$  points, the fourth-order term in the Landau free energy is given as follows:

$$\begin{aligned}
 F^{(4)} = & d_1 M_{B_1^{(1)}} M_{B_1^{(2)}} M_{B_1^{(3)}} M_z \\
 & + d_2 (M_{B_1^{(2)}}^2 - M_{B_1^{(3)}}^2) M_{B_1^{(1)}} M_{A^{(1)}} \\
 & + d_2 (M_{B_1^{(3)}}^2 - M_{B_1^{(1)}}^2) M_{B_1^{(2)}} M_{A^{(2)}} \\
 & + d_2 (M_{B_1^{(1)}}^2 - M_{B_1^{(2)}}^2) M_{B_1^{(3)}} M_{A^{(3)}}, \quad (26)
 \end{aligned}$$

where  $M_{A^{(i)}}$  and  $M_{B_1^{(i)}}$  represent the magnetic order parameters having  $A^-$  and  $B_1^-$  symmetry with ordering vector  $\mathbf{k} = \mathbf{k}_{M^{(i)}}$ , respectively, and  $M_z$  represents the magnetic order parameter having  $A_2^-$  symmetry with ordering vector  $\mathbf{k} = \mathbf{0}$ , i.e., the order parameter with same symmetry for  $z$  component of net magnetization. The Eq. (26) clearly shows that uniform  $M_z$  can be finite in the triple- $\mathbf{k}$  magnetic states induced from single- $\mathbf{k}$  magnetic states having  $B_1^-$  symmetry, indicating the emergence of AHE  $\sigma_{xy} \neq 0$  in the ordered phase though  $M_z$  is not necessary to be finite. Note that magnetic toroidal dipole  $T_z$  can be finite with  $M_z$  since  $T_z$  belongs to the same  $A_2^-$ -IRREP of  $M_z$  in the present crystal structure having chiral point group  $D_6$ . The vortexlike arrangements of magnetic moments can be regarded as toroidal dipole moments [89,90], and this is consistent with the magnetic structure shown in Fig. 11(a). The existence of magnetic toroidal dipole moments allows the magneto-electric effect and nonreciprocal charge transport, and these macroscopic responses can be footprints of triple- $\mathbf{k}$  ordering in the present case.

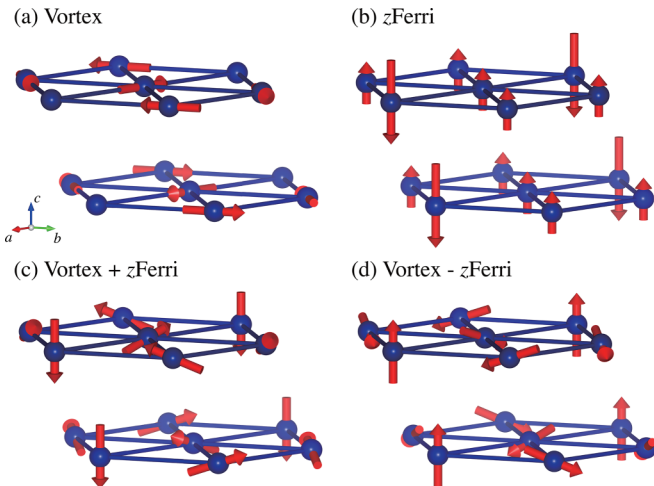


FIG. 12. Examples of linear combinations of triple- $\mathbf{k}$  states shown in Fig. 11.



As mentioned in the previous subsection, the electric order parameters are coupled with magnetic ones through the odd order terms in Landau free energy. The third-order terms are given as follows:

$$\begin{aligned}
F^{(3)} = & c_1(2M_{B_1^{(1)}}^2 - M_{B_1^{(2)}}^2 - M_{B_1^{(3)}}^2)Q_v \\
& + c_1\sqrt{3}(-M_{B_1^{(2)}}^2 + M_{B_1^{(3)}}^2)Q_{xy} \\
& + c_2M_{B_1^{(2)}}M_{B_1^{(3)}}Q_{A^{(1)}} \\
& + c_2M_{B_1^{(3)}}M_{B_1^{(1)}}Q_{A^{(2)}} \\
& + c_2M_{B_1^{(1)}}M_{B_1^{(2)}}Q_{A^{(3)}}, \tag{27}
\end{aligned}$$

where  $(Q_{xy}, Q_v)$  is the electric multipole having  $E_2^+$ -symmetry with propagation vector  $\mathbf{k} = \mathbf{0}$  and  $Q_{A^{(i)}}$  represents electric order parameter having  $A^+$ -symmetry with  $\mathbf{k} = \mathbf{k}_{M^{(i)}}$ . We can see that, from Eq. (27), single- $\mathbf{k}$  magnetic state  $M_{B_1^{(1)}} \neq 0$  and  $M_{B_1^{(2)}} = M_{B_1^{(3)}} = 0$  breaks the crystallographic point group from hexagonal group  $D_6$  to orthorhombic one  $D_2$  and leads to the emergence of the secondary electric order parameter  $Q_v$ . The triple- $\mathbf{k}$  state,  $M_{B_1^{(2)}} = M_{B_1^{(1)}} = M_{B_1^{(3)}} \neq 0$ , preserves the crystallographic point group  $D_6$ , and the electric multipoles with  $\mathbf{k} = \mathbf{0}$  are not induced as a result. Note that the unit cell in the triple- $\mathbf{k}$  state is extended in the  $ab$ -plane from the nonmagnetic one though the triple- $\mathbf{k}$  state has the same crystallographic point group with that for the nonmagnetic state. The resulting finite components of macroscopic response tensors associated with electric order parameters are thus unchanged from those in the paramagnetic phase. Meanwhile, the electric order parameters with  $\mathbf{k} = \mathbf{k}_{M^{(i)}}$  emerges  $Q_{A^{(1)}} = Q_{A^{(2)}} = Q_{A^{(3)}} \neq 0$ . These order parameters  $Q_{A^{(i)}}$  corresponds to charge ordering with the propagation vector  $\mathbf{k}_{M^{(i)}}$  and can be measured by the microscopic probes such as x-ray diffraction measurements. Thus the secondary order parameters are useful for gaining information about primary order ones also in this case.

#### IV. SUMMARY AND OUTLOOK

We have proposed a generation method of symmetry-adapted magnetic structure basis set with finite propagation vector  $\mathbf{k}$  based on the multipole expansion. In this method, the magnetic configurations on a virtual cluster of each propagation vector is first generated with use of the multipole expansion and then these are mapped onto crystallographic systems with a phase factor to take into consideration of spatial modulation of magnetic structures specified by a wave vector  $\mathbf{k}$ . The iterative implementation of this procedure with Gram-Schmidt orthogonalization provides complete orthonormal magnetic bases with a given  $\mathbf{k}$  classified according to irreducible representations under  $\mathbf{k}$ -group in arbitrary crystal structures. We can also construct the multi- $\mathbf{k}$  magnetic structures as the induced representation of the single- $\mathbf{k}$  states. The obtained magnetic structures can be good candidates for initial magnetic configurations for density functional theory (DFT) calculations [12] and thus high-throughput DFT calculations for magnetic materials combined with the present magnetic basis generation method is a possible future direction of our work.

Another potential application is a systematic analysis of the neutron scattering data. Magnetic structures generated in the present scheme form complete basis set and thus can be used for fitting of neutron diffraction patterns to identify magnetic structures. The detailed characterization of neutron scattering data of complicated magnetic structures with the use of magnetic bases based on the multipole expansion is an interesting future issue.

The present method is applied to representative materials  $\alpha$ -Mn and  $\text{CoM}_3\text{S}_6$  ( $M = \text{Nb}, \text{Ta}$ ) showing large anomalous Hall effect (AHE) with tiny net magnetization, whose magnetic structures are not clarified experimentally. It is demonstrated that magnetic structures compatible with both AHE and small ferromagnetic moment can be constructed. We also discuss the secondary order parameter, physical responses, and electronic properties under magnetic orders in  $\alpha$ -Mn and  $\text{CoM}_3\text{S}_6$ . We show that various phenomena such as AHE, anomalous Nernst effect (ANE), and magneto-optical Kerr effect (MOKE) can emerge through the primary magnetic order parameter having  $T_1^-$  symmetry with  $\mathbf{k} = \mathbf{0}$  for the high-pressure phase in  $\alpha$ -Mn, and the Edelstein effect driven by the odd parity electric order parameters are possible both in the ambient and high-pressure phases since the symmetry of secondary electric order parameters are same in both phases. For  $\text{CoM}_3\text{S}_6$ , the magnetic order parameter with  $T_1^-$ -symmetry with  $\mathbf{k} = \mathbf{0}$  are induced as a secondary order parameter in triple- $\mathbf{k}$  state, leading to emergence of AHE, ANE, MOKE, and nonreciprocal charge transport.

Our method is applicable to general magnets including noncollinear and noncoplanar antiferromagnets and skyrmion crystals [13]. The present magnetic structure generation scheme thus would facilitate exploration of functional magnetic materials.

#### ACKNOWLEDGMENTS

The authors thank K. Akiba, T. C. Kobayashi, S. Araki, H. Fukazawa, N. Shioda, T. Ohama, and Y. Kohori for fruitful discussions on experimental data for  $\alpha$ -Mn. They are also grateful to S. Seki, H. Takagi, and S. Minami for collaborative research on  $\text{CoM}_3\text{S}_6$ . This research was supported by JSPS KAKENHI Grants No. JP15H05883 (J-Physics), No. JP18H04230 (Topological Materials Science), No. JP19H01842, No. JP19H05825 (Quantum Liquid Crystals), No. JP20H05262 (Hypermaterials), No. JP20K05299, No. JP20K21067, No. JP21H01031, No. JP21H01789, No. JP21H04437, No. JP21H04990, and No. JP22H00290, by JST PRESTO Grants No. JPMJPR17N8 and No. JPMJPR20L7, and by JST-Mirai Program Grant No. JPMJMI20A1. They acknowledge Center for Computational Materials Science, Institute for Materials Research, Tohoku University for the use of MASAMUNE-IMR. Figures of crystal and magnetic structures are created by using VESTA [91].

#### APPENDIX: TRANSFORMATION PROPERTIES OF $\Psi_{\Gamma_k\gamma}$

In this Appendix, we show that  $\Psi_{\Gamma_k\gamma}^{(X)}$  in Eq. (15) belongs to  $\Gamma_k$ -IRREP. Since magnetic bases on virtual cluster  $\tilde{\Psi}_{\Gamma_k\gamma}$  have transformation properties of IRREP  $\Gamma_k$ , we should show the following relation:  $\{p_i h_\zeta | \tau_i\} \Psi_{\Gamma_k\gamma}^{(X)} =$



$\sum_{\gamma'} D_{\gamma'\gamma}^{\Gamma_k}(\{p_i h_\zeta | \tau_i\}) \Psi_{\Gamma_k \gamma'}^{(X)}$ , where  $\{p_i h_\zeta | \tau_i\} \in \mathcal{G}_k$ . The basis  $e_{k\alpha\mu}^{\text{axial}}$  have the following transformation properties under a  $k$ -group operation  $\{p_i h_\zeta | \tau_i\}$ ,

$$\{p_i h_\zeta | \tau_i\} e_{k\alpha\mu}^{\text{axial}} = \sum_{\nu} D_{\nu\mu}^{(\text{axial})}(p_i h_\zeta) e^{-i\varphi_{i\zeta}^{k,\alpha}} e_{k s_{i\zeta}^{[\alpha]}\nu}^{\text{axial}}, \quad (\text{A1})$$

where  $D^{(\text{axial})}$  is the transformation matrix of axial vector. We here note that the following relation for  $R_{i\zeta}^{s_{i\zeta}^{[\alpha]}}$  is satisfied,

$$\begin{aligned} R_{i\zeta}^{s_{i\zeta}^{[\alpha]}} &= \{p_i h_\zeta | \tau_i\} \eta_{s_{i\zeta}^{[\alpha]}} - \eta_{s_{i\zeta}^{[s_{i\zeta}^{[\alpha]}]}} \\ &= \{p_i h_\zeta | \tau_i\} \{p_{i'} h_{\zeta'} | \tau_{i'}\} \eta_\alpha - p_i h_\zeta R_{i\zeta}^\alpha - \eta_{s_{i\zeta}^{[\alpha]}} \\ &= \{p_{i'} h_{\zeta'} | \tau_{i'}\} \eta_\alpha + \mathbf{T} - p_i h_\zeta R_{i\zeta}^\alpha - \eta_{s_{i\zeta}^{[\alpha]}}, \end{aligned} \quad (\text{A2})$$

where symmetry operation  $p_{i'} h_{\zeta'}$  and a primitive translation  $\mathbf{T}$  are given as follows:

$$p_{i'} h_{\zeta'} = p_i h_\zeta p_{i'} h_{\zeta'}, \quad (\text{A3})$$

$$\mathbf{T} = p_i h_\zeta \tau_{i'} + \tau_i - \tau_{i'}. \quad (\text{A4})$$

By taking account of the relations in Eqs. (A2)–(A4), it is shown that  $\{p_i h_\zeta | \tau_i\} \Psi_{\Gamma_k \gamma}^{(X)}$  is written as follows:

$$\begin{aligned} \{p_i h_\zeta | \tau_i\} \Psi_{\Gamma_k \gamma}^{(X)} &= \sum_{i'=1}^{N_{\text{coset}}} \sum_{\zeta'=1}^{N_h} \sum_{\mu, \nu} e^{-i\varphi_{i'\zeta'}^{k,1} - i\mathbf{k} \cdot \mathbf{T}} \\ &\quad \times D_{\mu\nu}^{(\text{axial})}(p_i h_\zeta) u_{k\Gamma\gamma, i'\zeta'}^{(X)} e_{k s_{i'\zeta'}^{[1]}\mu}^{\text{axial}}. \end{aligned} \quad (\text{A5})$$

Let us here derive the relation among  $D_{\gamma'\gamma}^{\Gamma_k}$ ,  $D_{\mu\nu}^{(\text{axial})}$ , and  $u_{k\Gamma\gamma, \alpha\nu}^{(X)}$  from the transformation properties of magnetic bases on virtual cluster  $\tilde{\Psi}_{\Gamma_k \gamma}^{(X)}$ . Similarly to Eq. (A1), the magnetic bases  $\tilde{e}_{k i' \zeta' \mu}^{\text{axial}}$  are transformed under a symmetry operation

$\{p_i h_\zeta | \tau_i\}$  as follows:

$$\{p_i h_\zeta | \tau_i\} \tilde{e}_{k i' \zeta' \mu}^{\text{axial}} = \sum_{\nu} D_{\nu\mu}^{(\text{axial})}(p_i h_\zeta) e^{-i\tilde{\varphi}_{i'\zeta'}^{k, i' \zeta'}} \tilde{e}_{k i' \zeta' \nu}^{\text{axial}}, \quad (\text{A6})$$

where the phase factor is given as  $\tilde{\varphi}_{i'\zeta'}^{k, i' \zeta'} = \mathbf{k} \cdot \tilde{\mathbf{R}}_{i'\zeta'}^{i' \zeta'}$  with  $\tilde{\mathbf{R}}_{i'\zeta'}^{i' \zeta'} = \{p_i h_\zeta | \tau_i\} \tilde{\eta}_{i'\zeta'} - \tilde{\eta}_{i'\zeta'}$ . We here use the definition of virtual cluster described in Sec. II B, that is,  $\tilde{\eta}_{i'\zeta'} = \{p_{i'} h_{\zeta'} | \tau_{i'}\} \mathbf{r}_1$  and the relation in Eq. (A3). Therefore the magnetic basis  $\tilde{\Psi}_{\Gamma_k \gamma}^{(X)}$  shows following transformation properties:

$$\begin{aligned} \{p_i h_\zeta | \tau_i\} \tilde{\Psi}_{\Gamma_k \gamma}^{(X)} &= \sum_{i'=1}^{N_{\text{coset}}} \sum_{\zeta'=1}^{N_h} \sum_{\mu\nu} D_{\mu\nu}^{(\text{axial})}(p_i h_\zeta) \\ &\quad \times e^{-i\tilde{\varphi}_{i'\zeta'}^{k, i' \zeta'}} u_{k\Gamma\gamma, i'\zeta'}^{(X)} \tilde{e}_{k i' \zeta' \mu}^{\text{axial}}. \end{aligned} \quad (\text{A7})$$

By considering the relation  $\{p_i h_\zeta | \tau_i\} \tilde{\Psi}_{\Gamma_k \gamma}^{(X)} = \sum_{\gamma'} D_{\gamma'\gamma}^{\Gamma_k}(\{p_i h_\zeta | \tau_i\}) \tilde{\Psi}_{\Gamma_k \gamma'}^{(X)}$ , as well as Eq. (A7), we can obtain the following relation:

$$\begin{aligned} \sum_{\nu} D_{\mu\nu}^{(\text{axial})}(p_i h_\zeta) u_{k\Gamma\gamma, \alpha\nu}^{(X)} e^{-i\tilde{\varphi}_{i'\zeta'}^{k, i' \zeta'}} \\ = \sum_{\gamma'} D_{\gamma'\gamma}^{\Gamma_k}(\{p_i h_\zeta | \tau_i\}) u_{k\Gamma\gamma', i'\zeta'}^{(X)}. \end{aligned} \quad (\text{A8})$$

Putting Eq. (A8) into Eq. (A5), we obtain the following relation:

$$\begin{aligned} \{p_i h_\zeta | \tau_i\} \Psi_{\Gamma_k \gamma}^{(X)} &= \sum_{\gamma'} \sum_{i'=1}^{N_{\text{coset}}} \sum_{\zeta'=1}^{N_h} \sum_{\mu} e^{-i\varphi_{i'\zeta'}^{k,1} - i\mathbf{k} \cdot \mathbf{T} + i\tilde{\varphi}_{i'\zeta'}^{k, i' \zeta'}} \\ &\quad \times D_{\gamma'\gamma}^{\Gamma_k}(\{p_i h_\zeta | \tau_i\}) u_{k\Gamma\gamma', i'\zeta'}^{(X)} e_{k s_{i'\zeta'}^{[1]}\mu}^{\text{axial}}. \end{aligned} \quad (\text{A9})$$

Using the relations in Eqs. (A3) and (A4) and following the same manner of calculation in Eq. (A2), we can show that  $\tilde{\mathbf{R}}_{i'\zeta'}^{i' \zeta'} = \mathbf{T}$  and  $\tilde{\varphi}_{i'\zeta'}^{k, i' \zeta'} = \mathbf{k} \cdot \mathbf{T}$ . Consequently, the relation  $\{p_i h_\zeta | \tau_i\} \Psi_{\Gamma_k \gamma}^{(X)} = \sum_{\gamma'} D_{\gamma'\gamma}^{\Gamma_k}(\{p_i h_\zeta | \tau_i\}) \Psi_{\Gamma_k \gamma'}^{(X)}$  holds and thus, the magnetic basis  $\Psi_{\Gamma_k \gamma}^{(X)}$  belongs to  $\Gamma_k$ -IRREP under  $k$ -group  $\mathcal{G}_k$ .

[1] M.-T. Suzuki, T. Koretsune, M. Ochi, and R. Arita, *Phys. Rev. B* **95**, 094406 (2017).  
 [2] M.-T. Suzuki, T. Nomoto, R. Arita, Y. Yanagi, S. Hayami, and H. Kusunose, *Phys. Rev. B* **99**, 174407 (2019).  
 [3] M.-T. Suzuki, H. Ikeda, and P. M. Oppeneer, *J. Phys. Soc. Jpn.* **87**, 041008 (2018).  
 [4] S. Nakatsuji, N. Kiyohara, and T. Higo, *Nature (London)* **527**, 212 (2015).  
 [5] M. Ikhlas, T. Tomita, T. Koretsune, M.-T. Suzuki, D. Nishio-Hamane, R. Arita, Y. Otani, and S. Nakatsuji, *Nat. Phys.* **13**, 1085 (2017).  
 [6] T. Higo, H. Man, D. B. Gopman, L. Wu, T. Koretsune, O. M. J. van't Erve, Y. P. Kabanov, D. Rees, Y. Li, M.-T. Suzuki, S. Patankar, M. Ikhlas, C. L. Chien, R. Arita, R. D. Shull, J. Orenstein, and S. Nakatsuji, *Nat. Photonics* **12**, 73 (2018).  
 [7] R. Karplus and J. M. Luttinger, *Phys. Rev.* **95**, 1154 (1954).

[8] S. V. Gallego, J. M. Perez-Mato, L. Elcoro, E. S. Tasci, R. M. Hanson, K. Momma, M. I. Aroyo, and G. Madariaga, *J. Appl. Crystallogr.* **49**, 1750 (2016).  
 [9] E. F. Bertaut, *Acta Crystallogr. Sect. A* **24**, 217 (1968).  
 [10] Y. A. Izyumov, V. E. Naish, and R. P. Ozerov, *Neutron Diffraction of Magnetic Materials* (Consultants Bureau, New York, 1991).  
 [11] C. J. Bradley and A. P. Cracknell, *The Mathematical Theory of Symmetry in Solids: Representation Theory for Point Groups and Space Groups* (Oxford University Press, Oxford, 1972).  
 [12] M.-T. Huebsch, T. Nomoto, M.-T. Suzuki, and R. Arita, *Phys. Rev. X* **11**, 011031 (2021).  
 [13] N. Nagaosa and Y. Tokura, *Nat. Nanotechnol.* **8**, 899 (2013).  
 [14] H. T. Stokes, D. M. Hatch, and J. D. Wells, *Phys. Rev. B* **43**, 11010 (1991).

- [15] Z. L. Davies and A. S. Wills, *Adv. Condens. Matter Phys.* **2016**, 3960145 (2016).
- [16] J. D. Jackson, *Classical Electrodynamics* (Wiley, New York, 1999).
- [17] C. Schwartz, *Phys. Rev.* **97**, 380 (1955).
- [18] V. Dubovik and V. Tugushev, *Phys. Rep.* **187**, 145 (1990).
- [19] D. A. Varshalovich, A. N. Moskalev, and V. K. Khersonskii, *Quantum Theory of Angular Momentum* (World Scientific, Singapore, 1988).
- [20] H. Kusunose, *J. Phys. Soc. Jpn.* **77**, 064710 (2008).
- [21] The present treatment of magnetic moments, where spin moment is only considered is merely for simplifying the procedure of magnetic structure generation. The magnetic structures obtained by the present scheme does not cause any difficulty for practical applications such as symmetry analysis of physical phenomena and initial guess of magnetic structures in *ab initio* electronic structure calculations.
- [22] S. Hayami, M. Yatsushiro, Y. Yanagi, and H. Kusunose, *Phys. Rev. B* **98**, 165110 (2018).
- [23] O. V. Kovalev, *Representations of the Crystallographic Space Groups: Irreducible Representations, Induced Representations, and Corepresentations* (Gordon and Breach Science, Switzerland, 1993).
- [24] T. Inui, Y. Tanabe, and Y. Onodera, *Group Theory and Its Applications in Physics* (Springer-Verlag, Berlin, 1990).
- [25] In other words, we decompose a virtual cluster obtained by the method in Ref. [2] into  $N_{\text{coset}}$  clusters by shifting those atomic positions  $p_i, h_j, r_1$  by  $\tau_i$ .
- [26] K. Kubo and P. Thalmeier, *J. Phys. Soc. Jpn.* **78**, 083704 (2009).
- [27] C.-C. Lee, W.-G. Yin, and W. Ku, *Phys. Rev. Lett.* **103**, 267001 (2009).
- [28] J. Kouvel and J. Kasper, *J. Phys. Chem. Solids* **24**, 529 (1963).
- [29] H. Umebayashi and Y. Ishikawa, *J. Phys. Soc. Jpn.* **21**, 1281 (1966).
- [30] Y. Endoh and Y. Ishikawa, *J. Phys. Soc. Jpn.* **30**, 1614 (1971).
- [31] P. Burllet, D. Bonnisseau, S. Quezel, J. Rossat-Mignod, J. Spirlet, J. Rébizant, and O. Vogt, *J. Magn. Magn. Mater.* **63-64**, 151 (1987).
- [32] J. Sanchez, P. Burllet, S. Quézel, D. Bonnisseau, J. Rossat-Mignod, J. Spirlet, J. Rebizant, and O. Vogt, *Solid State Commun.* **67**, 999 (1988).
- [33] P. Burllet, F. Bourdarot, J. Rossat-Mignod, J. Sanchez, J. Spirlet, J. Rebizant, and O. Vogt, *Phys. B: Condens. Matter* **180-181**, 131 (1992).
- [34] G. Lander and P. Burllet, *Phys. B: Condens. Matter* **215**, 7 (1995).
- [35] J. Rossat-Mignod, P. Burllet, S. Quezel, and O. Vogt, *Physica B+C* **102**, 237 (1980).
- [36] N. Magnani, R. Caciuffo, G. H. Lander, A. Hiess, and L.-P. Regnault, *J. Phys.: Condens. Matter* **22**, 116002 (2010).
- [37] J. Yamaura, K. Ohgushi, H. Ohsumi, T. Hasegawa, I. Yamauchi, K. Sugimoto, S. Takeshita, A. Tokuda, M. Takata, M. Udagawa, M. Takigawa, H. Harima, T. Arima, and Z. Hiroi, *Phys. Rev. Lett.* **108**, 247205 (2012).
- [38] T.-h. Arima, *J. Phys. Soc. Jpn.* **82**, 013705 (2013).
- [39] P. Burllet, J. Rossat-Mignod, S. Quezel, O. Vogt, J. Spirlet, and J. Rebizant, *J. Less-Common Met.* **121**, 121 (1986).
- [40] K. Ikushima, S. Tsutsui, Y. Haga, H. Yasuoka, R. E. Walstedt, N. M. Masaki, A. Nakamura, S. Nasu, and Y. Ōnuki, *Phys. Rev. B* **63**, 104404 (2001).
- [41] S. B. Wilkins, R. Caciuffo, C. Detlefs, J. Rebizant, E. Colineau, F. Wastin, and G. H. Lander, *Phys. Rev. B* **73**, 060406(R) (2006).
- [42] G. H. Lander and R. Caciuffo, *J. Phys.: Condens. Matter* **32**, 374001 (2020).
- [43] M. Yatsushiro, H. Kusunose, and S. Hayami, *Phys. Rev. B* **104**, 054412 (2021).
- [44] S. Bigdeli, H. Mao, and M. Selleby, *Phys. Status Solidi B* **252**, 2199 (2015).
- [45] C. G. Shull and M. K. Wilkinson, *Rev. Mod. Phys.* **25**, 100 (1953).
- [46] T. Yamada, *J. Phys. Soc. Jpn.* **28**, 596 (1970).
- [47] T. Yamada, N. Kunitomi, Y. Nakai, D. E. Cox, and G. Shirane, *J. Phys. Soc. Jpn.* **28**, 615 (1970).
- [48] H. Yamagata and K. Asayama, *J. Phys. Soc. Jpn.* **33**, 400 (1972).
- [49] A. C. Lawson, A. C. Larson, M. C. Aronson, S. Johnson, Z. Fisk, P. C. Canfield, J. D. Thompson, and R. B. Von Dreele, *J. Appl. Phys.* **76**, 7049 (1994).
- [50] K. Takeda, A. Miyake, K. Shimizu, T. C. Kobayashi, and K. Amaya, *J. Phys. Soc. Jpn.* **77**, 025001 (2008).
- [51] K. Akiba, K. Iwamoto, T. Sato, S. Araki, and T. C. Kobayashi, *Phys. Rev. Res.* **2**, 043090 (2020).
- [52] T. Ito, H. Fukazawa, N. Shioda, Y. Kataoka, T. Ohama, and Y. Kohori, *J. Phys. Soc. Jpn.* **90**, 085001 (2021).
- [53] D. Hobbs and J. Hafner, *J. Phys.: Condens. Matter* **13**, L681 (2001).
- [54] D. Hobbs, J. Hafner, and D. Spišák, *Phys. Rev. B* **68**, 014407 (2003).
- [55] H. Ehteshami and P. A. Korzhavyi, *Phys. Rev. Mater.* **1**, 073803 (2017).
- [56] A. Pulkkinen, B. Barbiellini, J. Nokelainen, V. Sokolovskiy, D. Baigutlin, O. Miroshkina, M. Zagrebina, V. Buchelnikov, C. Lane, R. S. Markiewicz, A. Bansil, J. Sun, K. Pussi, and E. Lähderanta, *Phys. Rev. B* **101**, 075115 (2020).
- [57] N. Shioda, H. Fukazawa, T. Ohama, and Y. Kohori, *J. Phys. Soc. Jpn.* **91**, 023709 (2022).
- [58] H. Grimmer, *Acta Crystallogr., Sect. A* **49**, 763 (1993).
- [59] D. Gosálbez-Martínez, I. Souza, and D. Vanderbilt, *Phys. Rev. B* **92**, 085138 (2015).
- [60] H. Watanabe and Y. Yanase, *Phys. Rev. B* **98**, 245129 (2018).
- [61] S. Araki and T. C. Kobayashi (private communication).
- [62] H. Yan, O. Benton, L. Jaubert, and N. Shannon, *Phys. Rev. B* **95**, 094422 (2017).
- [63] The symmetry-adapted magnetic structures with  $\mathbf{k} = \mathbf{0}$  in pyrochlore systems having  $O_h$  point group symmetry are basically same as those in single tetrahedron having  $T_d$  point group symmetry. Note that IRREPs under  $O_h$  point group symmetry can be obtained by adding the subscript “g” to those under  $T_d$  point group symmetry such as  $A_2^- \rightarrow A_{2g}^-$  and  $T_{1g}^- \rightarrow T_{1g}^-$  from the compatibility relation between  $O_h$  and  $T_d$  point groups.
- [64] G. L. J. A. Rikken, J. Fölling, and P. Wyder, *Phys. Rev. Lett.* **87**, 236602 (2001).
- [65] G. L. J. A. Rikken and P. Wyder, *Phys. Rev. Lett.* **94**, 016601 (2005).
- [66] T. Ideue, K. Hamamoto, S. Koshikawa, M. Ezawa, S. Shimizu, Y. Kaneko, Y. Tokura, N. Nagaosa, and Y. Iwasa, *Nat. Phys.* **13**, 578 (2017).
- [67] K. Hamamoto, M. Ezawa, K. W. Kim, T. Morimoto, and N. Nagaosa, *Phys. Rev. B* **95**, 224430 (2017).

- [68] H. Watanabe and Y. Yanase, *Phys. Rev. Res.* **2**, 043081 (2020).
- [69] R. Oiwa and H. Kusunose, *J. Phys. Soc. Jpn.* **91**, 014701 (2022).
- [70] Strictly speaking, the second-order conductivity is composed of the following three contributions in the clean limit [68,69]: the Drude [66], Berry curvature dipole [92], and intrinsic terms [93]. All terms can be finite in the high-pressure magnetic phase of  $\alpha$ -Mn. We here focus on the Drude term, which is usually dominant in good metals without spatial inversion and time-reversal symmetries [43,66–69]. Another type of nonlinear charge transport, called nonlinear Hall effect characterized by the Berry curvature dipole term, can emerge even in the ambient pressure magnetic phase of  $\alpha$ -Mn due to the absence of inversion symmetry [92]. The charge currents induced by the nonlinear Hall effect are always perpendicular to an applied electric field [92], whereas the induced currents through the Drude term in the high-pressure magnetic phase are not orthogonal except for specific cases.
- [71] J.-C. Tolédano and P. Tolédano, *The Landau Theory of Phase Transitions, Application to Structural, Incommensurate, Magnetic and Liquid Crystal Systems* (World Scientific, Singapore, 1987).
- [72] G. Y. Lyubarskii, *The Application of Group Theory in Physics* (Pergamon Press, Oxford, 1960).
- [73] R. Shiina, H. Shiba, and P. Thalmeier, *J. Phys. Soc. Jpn.* **66**, 1741 (1997).
- [74] R. Shiina, O. Sakai, H. Shiba, and P. Thalmeier, *J. Phys. Soc. Jpn.* **67**, 941 (1998).
- [75] Y. Kuramoto, H. Kusunose, and A. Kiss, *J. Phys. Soc. Jpn.* **78**, 072001 (2009).
- [76] M.-T. Suzuki and H. Ikeda, *Phys. Rev. B* **90**, 184407 (2014).
- [77] R. R. Birss, *Symmetry and Magnetism* (North-Holland, Amsterdam, 1964).
- [78] L. S. Levitov, Y. V. Nazarov, and G. M. Éliashberg, *Zh. Eksp. Teor. Fiz.* **88**, 229 (1985) [*Sov. Phys. JETP* **61**, 133 (1985)].
- [79] V. M. Edelstein, *Solid State Commun.* **73**, 233 (1990).
- [80] S. Zhong, J. E. Moore, and I. Souza, *Phys. Rev. Lett.* **116**, 077201 (2016).
- [81] Y. Togawa, T. Koyama, K. Takayanagi, S. Mori, Y. Kousaka, J. Akimitsu, S. Nishihara, K. Inoue, A. S. Ovchinnikov, and J. Kishine, *Phys. Rev. Lett.* **108**, 107202 (2012).
- [82] Y. Togawa, Y. Kousaka, K. Inoue, and J.-i. Kishine, *J. Phys. Soc. Jpn.* **85**, 112001 (2016).
- [83] T. Inoshita, M. Hirayama, N. Hamada, H. Hosono, and S. Murakami, *Phys. Rev. B* **100**, 121112(R) (2019).
- [84] N. J. Ghimire, A. S. Botana, J. S. Jiang, J. Zhang, Y. S. Chen, and J. F. Mitchell, *Nat. Commun.* **9**, 3280 (2018).
- [85] G. Tenasini, E. Martino, N. Ubrig, N. J. Ghimire, H. Berger, O. Zaharko, F. Wu, J. F. Mitchell, I. Martin, L. Forró, and A. F. Morpurgo, *Phys. Rev. Res.* **2**, 023051 (2020).
- [86] S. Mangelsen, P. Zimmer, C. Näther, S. Mankovsky, S. Polesya, H. Ebert, and W. Bensch, *Phys. Rev. B* **103**, 184408 (2021).
- [87] S. S. P. Parkin, E. A. Marseglia, and P. J. Brown, *J. Phys. C: Solid State Phys.* **16**, 2765 (1983).
- [88] M. Seemann, D. Ködderitzsch, S. Wimmer, and H. Ebert, *Phys. Rev. B* **92**, 155138 (2015).
- [89] N. A. Spaldin, M. Fiebig, and M. Mostovoy, *J. Phys.: Condens. Matter* **20**, 434203 (2008).
- [90] S. Hayami, H. Kusunose, and Y. Motome, *Phys. Rev. B* **90**, 024432 (2014).
- [91] K. Momma and F. Izumi, *J. Appl. Crystallogr.* **44**, 1272 (2011).
- [92] I. Sodemann and L. Fu, *Phys. Rev. Lett.* **115**, 216806 (2015).
- [93] Y. Gao, S. A. Yang, and Q. Niu, *Phys. Rev. Lett.* **112**, 166601 (2014).